

Markov Chain Model of Entanglement Setup in Noisy Dynamic LEO Satellite Networks

Yifan Gao Alvin Valera Winston K.G. Seah

School of Engineering and Computer Science

Victoria University of Wellington

Wellington, New Zealand

yifan.gao@vuw.ac.nz, {alvin.valera,winston.seah}@ecs.vuw.ac.nz

Abstract—Quantum entanglement routing in dynamic Low Earth Orbit (LEO) satellite networks is important for achieving scalable and high-fidelity quantum communication. However, the dynamic characteristics of satellite network topology, limited quantum resources and strict coherence time constraints pose significant challenges to reliable entanglement routing. An entanglement distribution analysis model for this unique environment is critical and helpful for entanglement routing research. We address the fundamental challenge of establishing and maintaining quantum entanglement links between satellites operating in free space, where links are subject to both transmission losses and quantum memory decoherence. This paper presents a comprehensive Markov chain model with a state space defined by link storage age and physical distance for analyzing entanglement distribution in noisy dynamic LEO satellite quantum networks. We construct transition matrices that capture system dynamics under varying request arrival rates, and derive analytical expressions for key performance metrics, including request satisfaction rate, average waiting time, link utilization efficiency, and average consumed link fidelity. Our analysis reveals that the critical trade-offs of higher request rates lead to faster link consumption with higher fidelity but potentially lower satisfaction rates, while lower request rates allow longer storage times at the cost of lower fidelity of increased decoherence effect. Moreover, this paper proves it is reasonable to leave out polarization rotation when the transmission distance is very short (40 – 50km). In summary, this work provides theoretical foundations for designing and optimizing quantum entanglement distribution strategies in satellite networks, with applications to global-scale quantum communications.

Index Terms—LEO satellite, Free Space, Markov Chains, Decoherence

I. INTRODUCTION

The quantum entanglement forms the foundation of quantum communication networks, with entangled states between spatially separated parties, enabling quantum key distribution (QKD) and distributed quantum computing. The quality of entanglement can be quantified by fidelity $F \in [0, 1]$, which must exceed a minimum application threshold F_{th} to be used. However, terrestrial quantum communication faces distance limitations due to exponential photon loss in optical fibers, and restricting direct quantum links to about 100 – 200km [1]. To overcome this distance drawback, we consider LEO satellites as the nodes of the quantum networks, which offer a solution by operating at altitudes between 200 – 2000km [2] where free space quantum channels have lower photon loss compared to optical fibers [3]–[6]. At altitudes above 200km,

atmospheric effects become negligible, so the dominant losses are geometric beam divergence and polarization rotation under this condition, and they can be modeled mathematically [7]. Meanwhile, LEO satellites can enable global quantum coverage because of their high flexibility and shorter transmission distance compared with Medium Earth Orbit (MEO) and Geostationary Earth Orbit (GEO) satellites [8].

However, LEO satellites also have some drawbacks because of rapid topology changing, they have high orbital velocities with short communication windows, limited to 5 – 15 minutes [9], [10]. And the satellite control limitations introduce the pointing errors that further reduce the photon capture probability [8], [11]. It is usually considered quantum memories aboard satellites to store the qubits, but they suffer from the decoherence effect in this equipment, which causes a gradual loss of quantum coherence due to environmental interactions [12]. The fidelity of stored entanglement degrades exponentially because this reason imposes a limited coherence time T_{cutoff} , which is the maximum storage duration before the fidelity drops below the minimum application threshold F_{th} [13]. Therefore, there is a fundamental trade-off between storing entanglement for future requests and generating new entanglement on demand. Meanwhile, satellite quantum networks operate under strict constraints on quantum memory capacity [14]. Also, the entanglement generation and photon transmission processes are probabilistic, which means they may fail [15]. These constraints distinguish satellite quantum networks from both classical satellite networks and terrestrial quantum networks, so satellite quantum networks require specialized analytical models.

So, we come up with the Markov chain, which is useful to model the time-varying processes of the probabilistic entanglement setup [16], [17]. While it has been successfully applied to analyze terrestrial quantum repeater chains [18], [19], existing models typically assume a fiber environment [20]–[22]. None of them hold for dynamic LEO satellite networks (to our best knowledge), where photons fly in free space, the topology changes continuously, varying transmit distances, and short communication windows. Therefore, we aim to design our unique analysis model of the entanglement setup processes of dynamic LEO satellite quantum networks under the noisy space environment.

Given a dynamic satellite quantum network in which satel-

lites continuously move beyond the minimum safety distance. Entangled links exist only between satellites within a maximum distance threshold. Every request for entanglement distribution arrives sequentially, with at most one request per time slot specifying source and destination satellites. This problem aims to determine the communication routes between source and destination satellites that maintain end-to-end (E2E) quantum fidelity above the minimum acceptable threshold. This problem aims to minimize the average latency and entangled-pair consumption. Meanwhile, this problem is subject to the constraints of limited quantum memory capacity, entangled link capacity, and coherence time. Also, the links will degrade due to decoherence during storage and must be discarded when their fidelity falls below the threshold.

This paper presents the first (to our best knowledge) comprehensive Markov chain model for dynamic LEO satellite quantum networks, introducing a novel two-dimensional state space capturing both storage age and physical distance. We derive closed-form analytical expressions for four critical performance metrics that reveal fundamental trade-offs in satellite quantum communication. Higher request rates lead to faster link consumption with higher fidelity but lower satisfaction rates if the success rate of generating entanglement is low, while lower request rates allow longer storage times at the cost of lower fidelity of increased decoherence effect. Moreover, our analysis establishes several practical design guidelines for the LEO quantum network: 1) The capture probability of receiving a photon reaches 65.27% at 40km with ideal pointing, degrading to 56.74-62.91% under realistic pointing errors, while initial fidelity ranges from 64.95% to 55.86% at 40km depending on system parameters; 2) The maximum one-hop transmission distance is 50km under realistic error conditions ($\varepsilon = 1 - 3\%$, $\sigma_{rotation} < 1\mu rad$, $\sigma_{\delta} = 0.5 - 1\mu rad$), with coherence time constrained to ≤ 0.224 seconds; 3) These findings demonstrate that minimum receiver aperture radius of 120mm is required for $F_{th} = 0.5$, with optimal performance at 150mm achieving $d_{max} = 50.78km$; 4) We prove that polarization rotation effects contribute negligible impact ($\approx 10^{-7}\%$ relative difference) on maximum transmission distance for short links, enabling simplified system design.

The rest of this paper is structured as follows. Section II surveys related work on Markov chains for quantum networks and free-space quantum communication. Section III presents our system model, including problem formulation, Markov chain construction, transition dynamics, and analytical performance metrics. Section IV evaluates the model with realistic LEO satellite parameters. Finally, section V concludes this paper.

II. RELATED WORKS

This section reviews existing research on Markov chain models for quantum networks and free-space quantum communication systems, highlighting the gaps our work addresses. While prior work has analyzed either terrestrial quantum networks or classical satellite communications, no existing model captures the unique challenges of dynamic LEO satellite quantum networks operating in noisy free-space environments.

A. Markov Chains

Markov chain models provide a mathematical framework for analyzing quantum entanglement distribution in quantum networks, which helps to understand these random processes and calculate the key performance measures. From 2019 to 2024, several papers have deployed Markov chains in quantum entanglement distribution in fiber and terrestrial environments, but they have the same drawbacks, in that they didn't consider the changing distances of nodes and the free space environment [16], [23], [24]. Vinay et al. (2019) [23] established important mathematical foundations by using Markov chains to study entanglement establishment time when generation succeeds probabilistically, demonstrating that secret key rate predictions can improve by three orders of magnitude compared to simpler analytical methods. Building on this foundation, Brand et al. (2020) [24] achieved a significant breakthrough by developing polynomial-time algorithms that can efficiently analyze repeater chains with thousands of links, handle protocols incorporating purification steps, and provide exact results with high precision, which is a substantial improvement over the exponential-time complexity of earlier approaches. More recently, Zang et al. (2024) [16] advanced the field by deriving closed-form expressions for throughput and latency in continuously operating repeater chains, eliminating the need for computationally expensive simulations and revealing how two-link chain analysis can inform understanding of longer chains.

Despite these important contributions, existing Markov chain models have the same critical limitations that prevent their application to LEO satellite quantum networks. Firstly, all prior works assume static network topologies with fixed inter-node distance. Vinay et al. focused on small and simple networks without considering distance variations [23], Brand et al. explicitly assumed all nodes remain in the same positions with constant distances [24], and Zang et al.'s analysis does not account for the continuously changing topology characteristic of satellite networks [16]. Secondly, the steady-state analysis employed by Zang et al. requires systems to operate long enough for state probabilities to stabilize, which works well for terrestrial networks but fails for LEO satellites, where communication windows last only 5 – 15 minutes and the cutoff time of entangled states for less than 1 minute, which is insufficient to reach a steady state [16]. Thirdly, all existing models were designed for fiber-based terrestrial environments and do not incorporate free-space channel characteristics such as beam divergence, pointing errors, polarization rotation, or distance-dependent transmission losses that are critical in satellite scenarios [16], [23], [24]. Finally, Brand et al.'s approach analyzes only the first entanglement created rather than supporting continuous operation, limiting its applicability to practical quantum networks requiring sustained entanglement distribution [24].

B. Entanglement Generation in Free Space

This paper considers free-space quantum communication through satellites to overcome the distance limitation of fiber

networks on the ground, and many works have developed this kind of research, especially using LEO satellites. Early experiments like [3]–[6], [25], [26] showed that satellite-based quantum communication is possible. Liao et al. (2017) [3] successfully demonstrated satellite-to-ground QKD from the Micius satellite at 500 km altitude, achieving secure key rates over distances far exceeding fiber-based systems and extended this work to long-distance free-space QKD in day-light conditions till the next year [6], [25]. Then in 2020, Pan et al. [4], [26] explored free-space quantum secure direct communication, and in 2024, Sisodia et al. [5] provided a comparative study of free-space optical (FSO)-QKD protocols under realistic free-space losses and device imperfections. These studies show that free-space channels have lower loss than fibers for long distances, but face challenges like beam spreading, pointing errors, polarization rotation, and atmospheric effects.

Before quantum exploration, classical FSO communication faced similar problems in the atmosphere. Lee and Chan (2004) [27] showed that spatial diversity at both transmitter and receiver provides substantial power gain for mitigating atmospheric turbulence, which causes signal fading in clear atmospheric optical channels. 7 years later, Puryear et al. (2011) [28]–[30] experimentally analyzed the time dynamics of coherent communication through turbulence, validating the use of two-state continuous-time Markov processes to model outage statistics and demonstrating that log-amplitude fluctuations can be modeled as Gauss-Markov random processes. This Markov approach helps us to model how channels change over time, though these models focus on ground-to-ground links in fiber, rather than satellite links in free space.

Therefore, understanding how qubits’ state changes when passing through free space is important for us to design the system. Some typical works show that atmospheric channels need detailed probability models to capture random transmittance changes, which is important for quantum communication [31]–[33]. Vasylyev et al. (2016) [31] derived the probability distribution for atmospheric transmittance, including beam wandering, beam shape deformation, and beam broadening effects, with their elliptic beam approximation model applying to weak, weak-to-moderate, and strong turbulence regimes. Building on this work, the same authors developed a comprehensive theory of atmospheric quantum channels based on the law of total probability in 2018 [32]. They derived the probability distribution of transmittance (PDT) by separating contributions from turbulence of beam wandering and beam-spot distortions, which result in PDT varying from log-negative Weibull to truncated log-normal distributions depending on channel characteristics. Later in 2023, Klen and Semenov [33] obtained PDT for different horizontal links via numerical simulations, introducing an empirical model based on the Beta distribution that shows good agreement for a wide range of channel parameters. But none of them consider polarization rotation in their models, which is one of the main drawbacks that reduces the initial fidelity of entangled pairs.

C. Challenges

In summary, despite progress in both classical and quantum free-space communication, there are several gaps in the current works. Firstly, classical turbulence models focus on ground fiber links, and quantum channel models usually assume fixed satellite positions or observe single links only. Secondly, although the atmospheric turbulence theories provide good models, but don’t consider the moving topology and routing challenges of LEO networks. Also, the Markov time models from classical work haven’t been adapted for quantum memory systems, where both distance and storage time affect link fidelity.

Therefore, our work addresses these gaps by developing a Markov chain model designed specifically for moving satellite quantum networks. We make distance a fundamental part of the model, analyze performance during short time windows realistic for satellite passes, separate transmission and storage decoherence properly, and derive analytical formulas for multiple performance metrics.

III. SYSTEM MODEL

This section presents our comprehensive Markov chain model for analyzing entanglement distribution in dynamic LEO satellite quantum networks. We consider a dynamic LEO satellite network with line or grid topology, where the physical graph is represented as $G^t = (V^t, U^t)$ with $V^t = v_0^t, v_1^t, v_2^t, \dots, v_n^t$ denoting the physical positions of satellites at time t and $U^t = u_0^t, u_1^t, u_2^t, \dots, u_n^t$ representing the network edges. Since satellite networks operate in three-dimensional space, each satellite position is given by $v_i^t = (x_i^t, y_i^t, z_i^t)$, and the physical distance between two satellites is their Euclidean distance $D_{v_c^t, v_f^t}^t = \sqrt{(x_c^t - x_f^t)^2 + (y_c^t - y_f^t)^2 + (z_c^t - z_f^t)^2}$. An entangled link between two satellites exists only if their Euclidean distance is at most the maximum distance threshold \mathcal{D}_{max} . The cumulative sequences of source and destination nodes for all requests up to time slot t are denoted by $\mathfrak{S} = \{\mathfrak{s}^0, \mathfrak{s}^1, \dots, \mathfrak{s}^t\}$ and $\mathfrak{D} = \{\mathfrak{d}^0, \mathfrak{d}^1, \dots, \mathfrak{d}^t\}$, where $\mathfrak{s}^t \in V^t$ and $\mathfrak{d}^t \in V^t$, with at most one new request $(\mathfrak{s}^t, \mathfrak{d}^t)$ arriving per time slot. The logical graph $\mathcal{G}^t = (V^t, \mathcal{E}^t)$ represents the entangled link conditions at time t , where $\mathcal{E}^t = e_0^t, e_1^t, e_2^t, \dots, e_k^t$ denotes the available entangled links. Although satellites are continuously moving, we assume \mathcal{G}^t remains stable within continuous time slots T . Given this dynamic network, the problem is to determine routes with end-to-end (E2E) fidelity satisfying $F \geq F_{th}$ while minimizing average latency and EPR pair consumption, subject to constraints of limited quantum memory capacity, limited entangled link capacity, and limited coherence time T_{cutoff} , where links exceeding T_{cutoff} are discarded as unusable.

A. Constructing the Markov decision process

1) *State space*: Here, as a simple start, like Fig. 1(a), assume there is no decoherence, which means the link fidelity doesn’t degrade over time. Also, assume the link capacity is

TABLE I: Comparison of Related Works

Categories	Markov Chains			Free space							Our work
	[23]	[24]	[16]	[27]	[28]–[30]	[3], [6]	[31], [32]	[4], [26]	[33]	[5]	
Free-space	×	×	×	✓	×	✓	✓	✓	✓	✓	✓
Dynamic topology	×	×	×	×	×	×	×	×	×	×	✓
Variable distance	×	×	×	×	×	×	×	×	×	×	✓
Decoherence	✓	✓	✓	N/A	✓	N/A	✓	N/A	✓	✓	✓
Polarization Rotation	×	×	×	✓	✓	✓	✓	✓	✓	✓	✓
Large networks	×	✓	✓	×	×	×	×	×	×	×	✓

1. Consider Node A generates an EPR pair inside, and sends one photon of this pair to Node B, to generate an EPR pair with Node A. Therefore, the typical event now is whether an entangled link exists or not, whether the photon can be captured by Node B's telescope, and how this entanglement can be affected by the lossy quantum free space channel and decoherence in quantum memory.

2) *Action space:*

a) *Request arriving:* At each time slot, only allow 0 or 1 requests to arrive. The timeline of an EPR pair can be described in Fig.1(b). If one request arrives, the system needs to respond to it with two steps. Node A generates an EPR pair, with initial fidelity F_0 and probability p , then sends one qubit to Node B through the noisy free space channel, the fidelity would drop with the transmit distance d , the transmittance of the channel η , and the polarization rotation $\sigma_{rotation}$. At Node B, it has the probability q to capture the qubit successfully, and assume the fidelity decreases to F'_0 . Then, the two qubits will be stored in the quantum memories, respectively in Node A and B, for $i \cdot \Delta t$ time slots, until they are used or are discarded.

The state space is:

$$S = \{(i_{store}, d_j) | i_{store} \in \{0, 1, 2, \dots, K(d_j)\}, d_j \in \mathcal{D}\} \quad (1)$$

where i_{store} is the storing age of the link in time slot, d_j is the physical distance of two nodes, $\mathcal{D} = \{d_1, d_2, \dots, d_M\}$, $j \in M$, and $K(d)$ is the maximum storage age under distance d_j . The state space size is $|S| = \sum_{d_j \in \mathcal{D}} (K(d_j) + 1)$, means the system can be at $|S|$ kinds of stated in total. State $(0, d_j)$ means there is no usable entangled link, and the latest request asked for distance d_j . State (i_{store}, d_j) , $i_{store} \geq 1$ means there is one usable entangled link with distance d_j , it has been kept in quantum memory for $i_{store} \cdot \Delta t$ time slots, and the link suffers $t_{trans}(d_j) = \frac{d_j}{c}$ time slots for transmission when it is be generated.

Therefore, we develop this process by analyzing 4 important phases:

- the probability q ;
- the polarization rotation of qubits $\sigma_{rotation}$;
- the decoherence in the free space channel;
- and the decoherence in quantum memory.

b) *Gaussian Beam Diffraction:* The probability (q) of capturing a photon is very important in free-space quantum communication with LEO satellites, because the capture range of the equipment on the satellite is limited. When sending a photon through free space at an altitude higher than 200km with a rarefied atmosphere or vacuum, which is much higher

than the atmosphere (0 – 100km), we ignore atmospheric absorption, scattering, and turbulence effects in this scenario. For a Gaussian beam in free space, the spot radius at the receiving plane is:

$$W(d) = W_0 \sqrt{1 + \left(\frac{\omega d}{\pi W_0^2} \right)^2} \quad (2)$$

where W_0 is the beam waist radius at the transmitter, and ω is the wavelength of a single photon, d is the transmission distance. A fundamental parameter of beam propagation is the Rayleigh length $d_{\mathcal{R}} = \frac{\pi W_0^2}{\omega}$, which indicates the position where the spot area doubles from the beam waist. It is the critical distance where the diffraction effect begins to become significant. While LEO inter-satellite communications are much longer than the Rayleigh length, therefore:

$$W(d) \approx \frac{\omega d}{\pi W_0} \quad (3)$$

which shows that the spot radius increases linearly with distance. The corresponding divergence angle is $\theta \approx \frac{\omega}{\pi W_0}$, therefore, the smaller the beam waist, the greater the divergence. The spot area can be calculated as $A_{beam} = \pi W^2(d) = \frac{\omega^2 d^2}{\pi W_0^2}$.

At the receiving end, giving the radius of the receiving aperture is R_{ap} , so the aperture area is $A_{ap} = \pi R_{ap}^2$. In an ideal situation, the light beam is centered on the receiver, the transmission is:

$$\eta = \frac{A_{ap}}{A_{beam}} = \frac{\pi^2 W_0^2 R_{ap}^2}{\omega^2 d^2} \quad (4)$$

but this assumes perfect alignment. In practice, we need to consider the intensity distribution of a Gaussian beam at the receiving plane:

$$I(r, d) = I_0 \frac{W_0^2}{W^2(d)} \exp\left(-\frac{2r^2}{W^2(d)}\right) \quad (5)$$

where r is the radial distance, which is the vertical distance from the central axis of the beam to a certain point, and $I_0 = I(r = 0, d = 0)$ is the peak intensity at the beam waist. After integrating over the receiving aperture, we have the transmittance as:

$$\begin{aligned} \eta &= \frac{\int_0^{R_{ap}} I(r, d) \cdot 2\pi r dr}{\int_0^\infty I(r, d) \cdot 2\pi r dr} \\ &= 1 - e^{-\frac{2R_{ap}^2}{W^2(d)}} \\ &= 1 - e^{-\frac{2\pi^2 W_0^2 R_{ap}^2}{\omega^2 d^2}} \end{aligned} \quad (6)$$

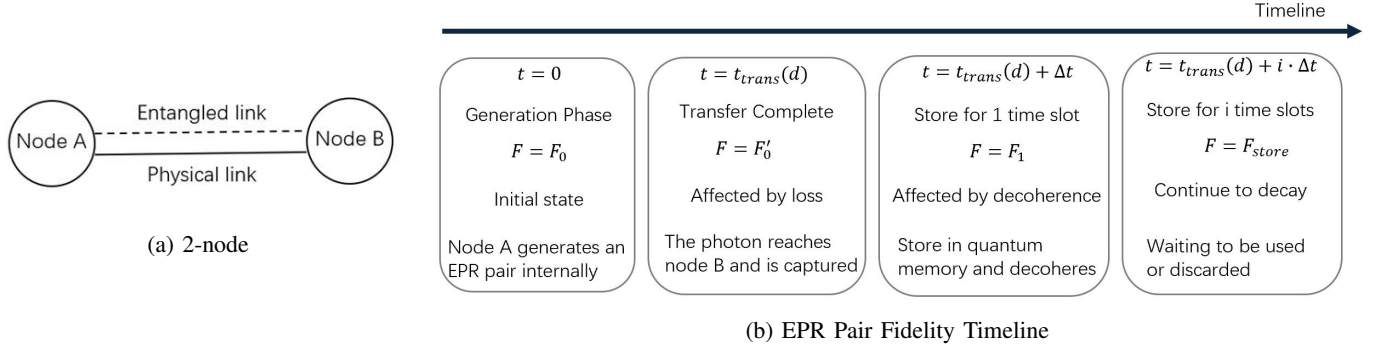


Fig. 1: Overall Illustration of the 2-node Configuration and Timeline

Meanwhile, due to the attitude control accuracy of LEO satellites being limited, so assume there is a pointing deviation δ (radians), and a beam center offset with distance $d_{deviation} = d \cdot \delta$. According to eq. 6, when there is no offset, that is, when the center of the beam is aligned with the center of the receiving aperture, the power in the receiving aperture is:

$$\varphi_{receive} = \int_0^{R_{ap}} I(r, d) \cdot 2\pi r dr \quad (7)$$

which gives us the geometric efficiency as eq. 6. Assume that the receiving aperture radius is much smaller than the spot radius, $R_{ap} \ll W(d)$, then the average light intensity within the aperture (I_{avg}) can be approximated as locally uniform in this circumstances, which means $I_{avg} \approx I(d_{deviation}, d)$. When the center of the beam is shifted as a distance $d_{deviation}$, and according to eq. 5, the light intensity at this position is attenuated relative to the axis as:

$$I(d_{deviation}, d) = I_0 \frac{W_0^2}{W^2(d)} \cdot e^{-\frac{2d_{deviation}^2}{W^2(d)}} \quad (8)$$

As the power collected by the aperture is proportional to this average light intensity, $\varphi_{receive} \propto I_{avg} \cdot \pi R_{ap}^2$, therefore, the attenuation factor relative to the no-offset case is:

$$\frac{\varphi_{receive}(d)}{\varphi_{receive}(0)} = e^{-\frac{2d_{deviation}^2}{W^2(d)}} \quad (9)$$

Therefore, the transmittance after considering the offset and eq. 6 is:

$$\begin{aligned} \eta_{derivation}(\delta) &= \eta \cdot e^{-\frac{2d_{deviation}^2}{W^2(d)}} \\ &= \eta \cdot e^{-\frac{2(d\delta)^2}{W^2(d)}} \\ &= \left[1 - e^{-\frac{2\pi^2 W_0^2 R_{ap}^2}{\omega^2 d^2}} \right] \cdot e^{-\frac{2d^2 \delta^2}{W^2(d)}} \end{aligned} \quad (10)$$

So, the larger the offset $d_{deviation} = d\delta$, the more severe the attenuation, and the larger the spot radius $W(d)$, and the higher the tolerance to offset.

c) *Pointing Error Effects*: Next, we need to calculate the average transmittance of random pointing errors. Assume the pointing deviation error δ follows a two-dimensional Gaussian distribution with a standard deviation σ_δ . Assume that the

pointing error components in two orthogonal directions are δ_x and δ_y , then the probability density function of the two-dimensional Gaussian distribution is:

$$P(\delta_x, \delta_y) = \frac{1}{2\pi\sigma_\delta^2} \cdot e^{-\frac{\delta_x^2 + \delta_y^2}{2\sigma_\delta^2}} \quad (11)$$

Here we assume that the errors in the two directions are independent and identically distributed. Since this problem has circular symmetry, because the transmittance depends only on the magnitude of the offset distance δ , and is independent of the direction, we convert the rectangular coordinates to polar coordinates as:

$$\begin{cases} \delta_x = \rho \cos \nu \\ \delta_y = \rho \sin \nu \end{cases} \quad (12)$$

where $\rho = \sqrt{\delta_x^2 + \delta_y^2}$ is the radial distance, which is the length of the offset, ν is the azimuth, and the Jacobian determinant is:

$$J = \begin{vmatrix} \frac{\partial x}{\partial r} & \frac{\partial x}{\partial \theta} \\ \frac{\partial y}{\partial r} & \frac{\partial y}{\partial \theta} \end{vmatrix} = \begin{vmatrix} \cos \theta & -\rho \sin \theta \\ \sin \theta & \rho \cos \theta \end{vmatrix} = \rho \quad (13)$$

The probability density function in polar coordinates becomes:

$$P(\rho, \nu) = P(\delta_x, \delta_y) \cdot |J| = \frac{1}{2\pi\sigma_\delta^2} \cdot e^{-\frac{\rho^2}{2\sigma_\delta^2}} \cdot \rho \quad (14)$$

Since the transmittance is independent of the azimuth angle ν , we integrate over ν from 0 to 2π and obtain the radial probability density function as Rayleigh distribution:

$$\begin{aligned} P(\rho) &= \int_0^{2\pi} p(\rho, \nu) d\nu = \int_0^{2\pi} \frac{\rho}{2\pi\sigma_\delta^2} \cdot e^{-\frac{\rho^2}{2\sigma_\delta^2}} d\nu \\ &= \frac{\rho}{2\pi\sigma_\delta^2} \cdot e^{-\frac{\rho^2}{2\sigma_\delta^2}} \cdot 2\pi = \frac{\rho}{\sigma_\delta^2} \cdot e^{-\frac{\rho^2}{2\sigma_\delta^2}} \end{aligned} \quad (15)$$

Since δ and ρ both represent the magnitude of the pointing error (i.e., $\delta = \rho = \sqrt{\delta_x^2 + \delta_y^2}$), we substitute $\delta = \rho$ into eq. 15 to maintain consistent notation throughout the derivation. Therefore, we get:

$$P(\delta) = \frac{\delta}{\sigma_\delta^2} \cdot e^{-\frac{\delta^2}{2\sigma_\delta^2}}, \delta \geq 0 \quad (16)$$

As the average transmittance is the expectation of the transmittance for all possible pointing errors, so $\langle \eta_{deviation} \rangle = \mathbb{E}[\eta_{deviation}(\delta)] = \int_0^\infty \eta_{deviation}(\delta) \cdot P(\delta) d\delta$, with eq. 10 and eq. 16, we have:

$$\begin{aligned} \langle \eta_{deviation} \rangle &= \int_0^\infty \cdot e^{-\frac{2d^2\delta^2}{W^2(d)}} \cdot \frac{\delta}{\sigma_\delta^2} \cdot e^{-\frac{\delta^2}{2\sigma_\delta^2}} d\delta \\ &= \frac{\eta}{\sigma_\delta^2} \int_0^\infty \delta e^{-\left(\frac{2d^2\delta^2}{W^2(d)} + \frac{\delta^2}{2\sigma_\delta^2}\right)} d\delta \quad (17) \\ &= \frac{\eta}{\sigma_\delta^2} \int_0^\infty \delta e^{-\delta^2 \left(\frac{2d^2}{W^2(d)} + \frac{1}{2\sigma_\delta^2}\right)} d\delta \end{aligned}$$

To simplify this, define a new coefficient ϵ as $\epsilon = \frac{2d^2}{W^2(d)} + \frac{1}{2\sigma_\delta^2}$, then:

$$\begin{aligned} \langle \eta_{deviation} \rangle &= \frac{\eta}{\sigma_\delta^2} \int_0^\infty \delta e^{-\epsilon\delta^2} d\delta = \frac{\eta}{\sigma_\delta^2} \cdot \frac{1}{2\epsilon} \\ &= \frac{\eta}{\sigma_\delta^2} \cdot \frac{1}{2 \left(\frac{2d^2}{W^2(d)} + \frac{1}{2\sigma_\delta^2}\right)} = \frac{\eta}{2\sigma_\delta^2 \left(\frac{2d^2}{W^2(d)} + \frac{1}{2\sigma_\delta^2}\right)} \\ &= \frac{\eta}{1 + \frac{4d^2\sigma_\delta^2}{W^2(d)}} \quad (18) \end{aligned}$$

To make this formula more concise, we define the attenuation factor β as $\beta = \frac{4d^2\sigma_\delta^2}{W^2(d)}$ to characterize the influence of pointing error relative to spot size, with eq. (3), we can get $\beta = \frac{4\pi^2 W_0^2 \sigma_\delta^2}{\omega^2}$. Therefore, the average transmittance at the receiver is:

$$\langle \eta_{deviation} \rangle = \frac{\eta}{1 + \beta}, \beta = \frac{4\pi^2 W_0^2 \sigma_\delta^2}{\omega^2} \quad (19)$$

As the conclusion, in the ideal condition, when pointing perfectly, the probability of successful single photon reception q is as eq. 6:

$$\begin{aligned} q_{ideal} &= \eta = 1 - e^{-\frac{2\pi^2 W_0^2 R_{ap}^2}{\omega^2 d^2}} \\ &= 1 - e^{-\frac{2R_{ap}^2}{\theta^2 d^2}} \quad (20) \end{aligned}$$

where $W_0 = \frac{\omega}{\pi\theta}$ is the beam waist radius at the transmitter, ω is the wavelength of a single photon, θ is the diverging half angle of this single photon light, d is the distance of two satellites, and R_{ap} is the radius of the receiving aperture. But in practice, if there exists a pointing error, then q_{error} is as eq. 19:

$$q_{error} = \frac{\eta}{1 + \beta} = \frac{1 - e^{-\frac{2R_{ap}^2}{\theta^2 d^2}}}{1 + \frac{4\sigma_\delta^2}{\theta^2}} \quad (21)$$

where $\theta = \omega/(\pi W_0)$ is the beam divergence half angle and σ_δ characterizes the pointing error standard deviation. Eq. (21) provides the capture probability accounting for both beam diffraction and geometric pointing errors.

d) Polarization Rotation in Moving Satellite Systems:

Now, we need to consider the qubit-state transformations that occur during transmission in this system. Fig. 2 shows the sender (Satellite A) transmitting the encoded quantum state

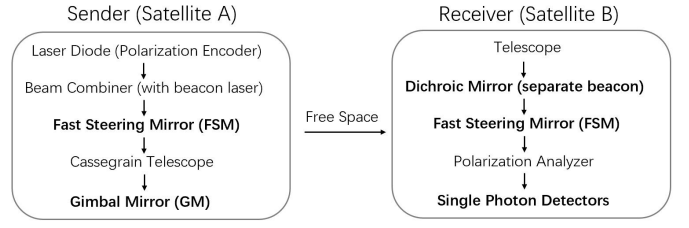


Fig. 2: Single Photon Path

photons through the Cassegrain telescope after precise pointing control by the fast steering mirror (FSM) and coarse adjustment by the Gimbal mirror, allowing them to propagate in free space. The receiver (Satellite B) collects the photons with a telescope, separates the beacon signal using the Dichroic mirror, performs precise tracking and correction using the FSM, and finally completes the quantum state measurement using a polarization analyzer and a single-photon detector [34]. In particular, the moving mirrors (bold font in this figure) within each satellite's pointing and tracking system introduce time-dependent polarization rotations that can severely degrade entanglement fidelity if left uncompensated. We now develop a comprehensive model for this critical quantum-level perturbation.

Consider a satellite moving along its orbit with velocity \vec{v}_{sat} , the pointing and tracking system employs FSMs that continuously adjust their orientation to maintain optical alignment between two satellites. Each mirror reflection introduces a coordinate transformation in the polarization basis. For a single mirror reflection, if the mirror normal makes an angle $\zeta(t)$ with respect to the optical axis at time t , and the plane of incidence rotates by angle $\vartheta(t)$ due to satellite motion, the polarization state experiences a rotation in the Bloch sphere [35]. The polarization state of a single photon can be represented in the computational basis $\{|H\rangle, |V\rangle\}$, which is the horizontal and vertical polarization, respectively. An arbitrary single-qubit state can be represented as:

$$|\phi\rangle = \cos\left(\frac{\chi}{2}\right) |H\rangle + e^{i\psi} \sin\left(\frac{\chi}{2}\right) |V\rangle \quad (22)$$

where $\chi \in [0, \pi]$ and $\psi \in [0, 2\pi]$ are the Bloch sphere angles. Then, we assume there is a polarization rotation by angle $\vartheta_{rotation}$ around an axis $\hat{\zeta} = (\zeta_x, \zeta_y, \zeta_z)$ on the Bloch sphere, which can be described by the rotation operator:

$$RO_{rotation}(\vartheta_{rotation}, \hat{\zeta}) = e^{-i \frac{\vartheta_{rotation}}{2} \hat{\zeta} \cdot \vec{Pauli}} \quad (23)$$

where $\vec{Pauli} = (Pauli_x, Pauli_y, Pauli_z)$ are the Pauli matrices:

$$Pauli_x = \begin{pmatrix} 0 & 1 \\ 1 & 0 \end{pmatrix}, Pauli_y = \begin{pmatrix} 0 & -i \\ i & 0 \end{pmatrix}, Pauli_z = \begin{pmatrix} 1 & 0 \\ 0 & -1 \end{pmatrix} \quad (24)$$

In the satellite scenario, the rotation is typically around an axis in the xy -plane, which is the linear polarization basis. The

rotation around the propagation axis can be described as [36]:

$$RO_{propagation}(\vartheta_{rotation}) = \begin{pmatrix} \cos(\vartheta_{rotation}) & -\sin(\vartheta_{rotation}) \\ \sin(\vartheta_{rotation}) & \cos(\vartheta_{rotation}) \end{pmatrix} \quad (25)$$

This transformation acts on the polarization state as:

$$\begin{pmatrix} \kappa_H \\ \kappa_V \end{pmatrix}_{out} = RO_{propagation}(\vartheta_{rotation}) \begin{pmatrix} \kappa_H \\ \kappa_V \end{pmatrix}_{in} \quad (26)$$

where κ_H and κ_V are the probability amplitudes for horizontal and vertical polarization, respectively.

After those, we need to consider the time when analyzing the rotation angle $\vartheta_{rotation}(t)$, because it is time-dependent and consists of systematic rotation $\vartheta_{systematic}(t)$ and random jitter $\vartheta_{jitter}(t)$. So, the time-dependent rotation angle can be described as:

$$\vartheta_{rotation}(t) = \vartheta_{systematic}(t) + \vartheta_{jitter}(t) \quad (27)$$

The first part arises from the predictable orbital motion, assuming a LEO satellite with orbital velocity v_{sat} and a communication window of duration t , the systematic rotation angle can be calculated as [37]:

$$\vartheta_{systematic}(t) = \frac{v_{sat}}{RE + h_{sat}} \cdot t \quad (28)$$

where $RE = 6371km$ is the Earth's radius, h_{sat} is the height of this satellite orbit.

The second part is caused by platform vibrations, attitude control errors, and mirror positioning uncertainties, which can be modeled as a zero-mean Gaussian random variable [38]:

$$\vartheta_{jitter}(t) \sim \mathcal{N}(0, \sigma_{rotation}^2) \quad (29)$$

where $\sigma_{rotation}$ is the standard deviation of the rotational jitter.

Then, we need to analyse the impact of polarization rotation on the fidelity of an EPR pair. For an ideal Bell state $|\Phi^+\rangle = \frac{|HH\rangle + |VV\rangle}{\sqrt{2}}$, the polarizations of the two photons are completely correlated. Here, if the first photon is horizontally polarized $|H\rangle$, then the second photon must also be $|H\rangle$; if the first is vertically polarized $|V\rangle$, then the second must also be $|V\rangle$. Assume photon 'a' travels from the transmitting node to the receiving node, undergoing a polarization rotation angle $\vartheta_{rotation}$ during transmission, while photon 'b' remains unchanged. We then apply the rotation operator $RO_{propagation}(\vartheta_{rotation})$ to photon 'a':

$$\begin{aligned} |\phi_{rotation}\rangle &= \frac{1}{\sqrt{2}} [(RO_{propagation}(\vartheta_{rotation}) \otimes I) |\Phi^+\rangle] \\ &= \frac{1}{\sqrt{2}} [\cos(\vartheta_{rotation}) |HH\rangle - \sin(\vartheta_{rotation}) |HV\rangle \\ &\quad + \sin(\vartheta_{rotation}) |VH\rangle + \cos(\vartheta_{rotation}) |VV\rangle] \end{aligned} \quad (30)$$

Where I is the identity operator, representing that photon 'b' is unchanged, and \otimes represents the tensor product. This equation shows that there were only two components ($|HH\rangle$ and $|VV\rangle$) in the completely correlated. But after rotation, the other two components $|HV\rangle$ and $|VH\rangle$ appear, which are the incompletely correlated. Moreover, the coefficients

$\cos(\vartheta_{rotation})$ and $\sin(\vartheta_{rotation})$ determine the weights of each component, when $\vartheta_{rotation} = 0$, it backs to the ideal Bell state, when $\vartheta_{rotation}$ larger, the rate of the bad components ($|HV\rangle$ and $|VH\rangle$) increases.

The fidelity after rotation of an EPR pair is defined as the degree to which a rotated state closely approximates the ideal state, which can be described as:

$$\begin{aligned} F_{rotation} &= |\langle \Phi^+ | \phi_{rotation} \rangle|^2 \\ &= \left| \frac{1}{\sqrt{2}} \langle HH + VV | [\cos(\vartheta_{rotation}) |HH\rangle - \sin(\vartheta_{rotation}) |HV\rangle + \sin(\vartheta_{rotation}) |VH\rangle + \cos(\vartheta_{rotation}) |VV\rangle] \right|^2 \\ &= \left| \frac{1}{2} [\cos(\vartheta_{rotation}) + 0 + 0 + \cos(\vartheta_{rotation})] \right|^2 \\ &= \cos^2(\vartheta_{rotation}) \\ &= \cos^2(\vartheta_{systematic} + \vartheta_{jitter}) \end{aligned} \quad (31)$$

Take the expectation of ϑ_{jitter} , we have:

$$\begin{aligned} \langle F_{rotation} \rangle &= \int_{-\infty}^{\infty} \cos^2(\vartheta_{systematic} + \vartheta_{jitter}) p(\vartheta_{jitter}) d\vartheta_{jitter} \\ &= \frac{1}{2} + \frac{1}{2} \int_{-\infty}^{\infty} \cos(2\vartheta_{systematic} + 2\vartheta_{jitter}) p(\vartheta_{jitter}) d\vartheta_{jitter} \\ &= \frac{1}{2} + \frac{1}{2} \cos(2\vartheta_{systematic}) \int_{-\infty}^{\infty} \cos(2\vartheta_{jitter}) p(\vartheta_{jitter}) d\vartheta_{jitter} \\ &\quad - \frac{1}{2} \sin(2\vartheta_{systematic}) \int_{-\infty}^{\infty} \sin(2\vartheta_{jitter}) p(\vartheta_{jitter}) d\vartheta_{jitter} \\ &= \frac{1}{2} [1 + \cos(2\vartheta_{systematic}) e^{-2\sigma_{rotation}^2}] \end{aligned} \quad (32)$$

Here, the angle brackets $\langle \cdot \rangle$ represent the expectation value operator. Specifically, $\langle F_{rotation} \rangle$ denotes the statistical average of the fidelity induced by rotation over all possible values of the Gaussian distributed jitter ϑ_{jitter} , weighted by their probability density function.

When calculating Gaussian integrals, we notice the first item of the second-to-last formula is an even function, so $\int \cos(2\vartheta_{jitter}) p(\vartheta_{jitter}) d\vartheta_{jitter} = e^{-2\sigma_{rotation}^2}$, the second item is an odd function with a zero mean distribution, so $\int \sin(2\vartheta_{jitter}) p(\vartheta_{jitter}) d\vartheta_{jitter} = 0$. Also, $p(\vartheta_{jitter}) = \frac{1}{\sqrt{2\pi\sigma_{rotation}^2}} \cdot e^{-\frac{\vartheta_{jitter}^2}{2\sigma_{rotation}^2}}$ is the Gaussian probability density function with standard deviation $\sigma_{rotation}$.

e) *Decoherence*: Now, we develop the effect of decoherence in the free space channel and quantum memory on the fidelity. The quantum state can only maintain a certain time (cutoff time) until it is affected by the noise channel and exponentially degrades to uselessness during storage in the quantum memory. Here, we assume that the low-fidelity entanglement will be discarded if its fidelity is lower than the minimum acceptable threshold, and all operations have to be completed within the limited cutoff time.

Decoherence in channel We have to know the fidelity of the entanglement when it is generated by Satellite A and is successfully captured by Satellite B through a travel through free space. [31]–[33] tells us that the transformation of the quantum state through the atmospheric channel is:

$$\Theta_{\text{out}}(\phi) = \int_0^1 d\eta \mathcal{P}(\eta) \frac{1}{\eta} \Theta_{\text{in}}\left(\frac{\phi}{\sqrt{\eta}}\right) \quad (33)$$

where $\Theta_{\text{in}}(\phi)$ is the input quantum states, $\Theta_{\text{out}}(\phi)$ is the output quantum states of the Glauber-Sudarshan quasiprobability distributions [39], [40]. $\mathcal{P}(\eta)$ is the probability distribution of the transmittance (PDT), and $\eta \in [0, 1]$ is the intensity transmittance we derived as Eq. (6).

In general cases, $\mathcal{P}(\eta)$ accounts for the random fluctuations in the free space channel. Various models exist for $\mathcal{P}(\eta)$, such as the Beta distribution for atmospheric turbulence scenarios [33]. However, for LEO satellite communication at altitudes higher than 200km, atmospheric effects are negligible, so the transmittance can become deterministic, and the fidelity after transmission can be directly calculated from the deterministic transmittance.

Meanwhile, the fidelity of the EPR pair is affected by the number of photon detection events. When the transmittance η decreases, the number of successfully received photons decreases, and the relative contribution of background noise and dark counts increases, which will lead to a decrease in the fidelity of the prepared EPR pair. According to the theory of quantum theory [41], when there exists loss, the fidelity of the Bell state can be described as:

$$F_0(\eta) = \frac{\eta + (1 - \eta) \cdot \varepsilon}{1 + 3(1 - \eta) \cdot \varepsilon} \quad (34)$$

Therefore, the initial fidelity after both polarization rotation (Eq. (32)) and transmission losses should be:

$$\begin{aligned} F'_0 &= \langle F_{\text{rotation}} \rangle \times F_0(\eta) \\ &= \frac{1}{2} \left[1 + \cos(2\vartheta_{\text{systematic}}) \cdot e^{-2\sigma_{\text{rotation}}^2} \right] \left[\frac{\eta + (1 - \eta) \cdot \varepsilon}{1 + 3(1 - \eta) \cdot \varepsilon} \right] \end{aligned} \quad (35)$$

If it costs time t to send a photon from satellite A to satellite B, then the time-dependent initial fidelity could become:

$$\begin{aligned} F'_0(t) &= \frac{1}{2} \left[1 + \cos(2\vartheta_{\text{systematic}}(t)) \cdot e^{-2\sigma_{\text{rotation}}^2} \right] \\ &\quad \times \left[\frac{\eta + (1 - \eta) \cdot \varepsilon}{1 + 3(1 - \eta) \cdot \varepsilon} \right] \\ &= \frac{1}{2} \left[1 + \cos\left(\frac{2v_{\text{sat}} \cdot t}{RE + h_{\text{sat}}}\right) e^{-2\sigma_{\text{rotation}}^2} \right] \\ &\quad \times \left[\frac{\eta + (1 - \eta) \cdot \varepsilon}{1 + 3(1 - \eta) \cdot \varepsilon} \right] \end{aligned} \quad (36)$$

where ε is the quantum bit error rate (QBER), caused by dark counts, background photons, and polarization rotation, v_{sat} is the orbital speed of the satellite, $RE = 6371\text{km}$ is the Earth's radius, h_{sat} is the height the this satellite orbit, and σ_{rotation} is the standard deviation of the rotational jitter.

Decoherence in quantum memory We model the decoherence in quantum memory using the amplitude damping channel, which describes energy dissipation and the spontaneous emission process [41]. For a single qubit stored for time t_{store} , the amplitude damping channel is characterized by Kraus operators:

$$KO_0 = \begin{bmatrix} 1 & 0 \\ 0 & \sqrt{1 - \alpha(t_{\text{store}})} \end{bmatrix}, \quad KO_1 = \begin{bmatrix} 1 & \sqrt{\alpha(t_{\text{store}})} \\ 0 & 0 \end{bmatrix} \quad (37)$$

where the damping probability is:

$$\alpha(t_{\text{store}}) = 1 - e^{-\Gamma t_{\text{store}}} \quad (38)$$

Here, Γ (unit: s^{-1}) is the damping rate that represents the strength of the coupling between the quantum memory and its environment.

For an EPR pair initially prepared in state $|\Phi^+\rangle = \frac{|00\rangle + |11\rangle}{\sqrt{2}}$ with initial fidelity F'_0 , both qubits are stored in quantum memories and experience amplitude damping independently. The amplitude damping affects the entangled state in two ways, 1) population transfer, $|11\rangle$ may decay to $|01\rangle, |10\rangle, |00\rangle$; 2) coherence loss can cause off-diagonal terms in the density matrix to decay.

After being stored for time t_{store} , the key observation is that the survival probability of both qubits remaining of both qubits remaining in their original state (without decay) is:

$$P_{\text{survive}} = (1 - \alpha(t_{\text{store}}))^2 = [e^{-\Gamma \cdot t_{\text{store}}}]^2 = e^{-2\Gamma \cdot t_{\text{store}}} \quad (39)$$

The fidelity of the stored EPR pair with respect to the target Bell state $|\Phi^+\rangle$ evolves as [21]:

$$F(t_{\text{store}}) = F'_0 \cdot P_{\text{survive}} = F'_0 \cdot e^{-2\Gamma \cdot t_{\text{store}}} \quad (40)$$

where F'_0 is the initial fidelity after transmission from eq (35), $t_{\text{store}} = i_{\text{store}} \cdot \Delta t$ is the total storing time. So the total age of an EPR pair t_{total} should be the sum of the transmission time t_{trans} and storage time t_{store} :

$$t_{\text{total}} = t_{\text{trans}} + t_{\text{store}} \quad (41)$$

and the cutoff time should include the transmission time, which means, given an application fidelity threshold F_{th} , which is the minimum acceptable fidelity for the quantum application, we can calculate the maximum lifetime T_{cutoff} of an EPR pair before it expires, which is the cutoff time:

$$\begin{aligned} F'_0(T_{\text{cutoff}} - t_{\text{trans}}) &= F_{\text{th}} \\ F'_0 \cdot e^{-2\Gamma \cdot (T_{\text{cutoff}} - t_{\text{trans}})} &= F_{\text{th}} \\ e^{-2\Gamma \cdot (T_{\text{cutoff}} - t_{\text{trans}})} &= \frac{F_{\text{th}}}{F'_0} \\ -2\Gamma \cdot (T_{\text{cutoff}} - t_{\text{trans}}) &= \ln \left[\frac{F_{\text{th}}}{F'_0} \right] \end{aligned} \quad (42)$$

$$T_{\text{cutoff}} = t_{\text{trans}} - \frac{1}{2\Gamma} \cdot \ln \left[\frac{F_{\text{th}}}{F'_0} \right]$$

$$T_{\text{cutoff}} = \frac{d}{c} - \frac{1}{2\Gamma} \cdot \ln \left[\frac{F_{\text{th}}}{F'_0} \right]$$

where c is the speed of light. Therefore, we can have the discrete maximum age K as:

$$K(d, F'_0) = \left\lfloor \frac{T_{\text{cutoff}}}{\Delta t} \right\rfloor = \left\lfloor \frac{d}{c\Delta t} - \frac{1}{2\Gamma\Delta t} \cdot \ln \left[\frac{F_{th}}{F'_0} \right] \right\rfloor \quad (43)$$

B. Transition Matrix

At each time slot t , one new request $(\mathfrak{s}^t, \mathfrak{d}^t)$ arrives, assuming the distance between the source node \mathfrak{s}^t and the destination node \mathfrak{d}^t is d_{new} . Assume the system responds to each request automatically, can not delay or deny, so the system must determine if there is a currently available link or not. If there is an available link ($i_{store} \geq 1$), then use it to satisfy the request, and the system transitions to a new state of trying to generate a new link. If no available link, they will try to generate a new link for the future request with distance d_{new} . So, no matter the previous state, the system will come to the state of trying to generate a new link.

Therefore, the transition of this system should consider the probability of a request arriving inside. Assume the probability of a request at each time slot is λ , then the comprehensive transition matrix of this system should be:

$$\mathcal{T} = \lambda \mathcal{T}_{d_{new}} + (1 - \lambda) \mathcal{T}_d \quad (44)$$

where $\mathcal{T}_{d_{new}}$ and \mathcal{T}_d are the transition matrices of this system under the conditions that there is a request and there is no request.

$$\mathcal{T}_{d_{new}} = \begin{bmatrix} 1-p' & p' & 0 & 0 & \cdots & 0 \\ 1-p' & p' & 0 & 0 & \cdots & 0 \\ 1-p' & p' & 0 & 0 & \cdots & 0 \\ \vdots & \vdots & \vdots & \vdots & \ddots & \vdots \\ 1-p' & p' & 0 & 0 & \cdots & 0 \end{bmatrix}_{(K+1) \times (K+1)} \quad (45)$$

$$\mathcal{T}_d = \begin{bmatrix} 1 & 0 & 0 & 0 & \cdots & 0 \\ 0 & 0 & 1 & 0 & \cdots & 0 \\ 0 & 0 & 0 & 1 & \cdots & 0 \\ \vdots & \vdots & \vdots & \vdots & \ddots & \vdots \\ 0 & 0 & 0 & 0 & \cdots & 1 \\ 1 & 0 & 0 & 0 & \cdots & 0 \end{bmatrix}_{(K+1) \times (K+1)} \quad (46)$$

where $p' = p \cdot q(d_{new}) \cdot P_{\text{success}}(d_{new})$ is the total probability of setting up an available link, $P_{\text{success}}(d_{new})$ is the probability of this link satisfying the minimum fidelity requirement. The matrix Eq. (45) means that when a request arrives, no matter the system state, the action will consume the link (if it has one) to satisfy the request, and try to generate a new link with distance d_{new} for the future request. Every line is the same in Eq.(45) because if the system is at state (i_{store}, d_{odd}) , then consume this link and try to generate a new one, if the system is at state $(0, d_{odd})$, then try generating a new link directly. For example, the first column means the system generates a new link that fails, transitions to state $(0, d_{new})$ with probability $1 - p'$. The second column means the system generates a new link successfully, transitions to state $(1, d_{new})$ with probability p' . Here, the system has a new link that ages 1 time slot. The

other columns are all 0 because the system can not transit to an older state without a link.

Meanwhile, the matrix Eq. (46) depicts the states without request, the system doesn't need to consume the link, but the link will age over time. The first line means if there is no link, then keep the state without link, the probability is $P_{(0,d) \rightarrow (0,d)} = 1$. The second to the K -th lines means if there is a link ages i time slots ($1 \leq i < K$), then aging for 1 time slot, the probabilities are $P_{(i,d) \rightarrow (i+1,d)} = 1$, and that's why the $(i+1)$ -th column the i -th line of Eq. (46) is 1, the others are 0. The last line means if the age of the link reaches the maximum storage time K , it should be discarded, with probability $P_{(K,d) \rightarrow (0,d)} = 1$.

1) *Fidelity Qualified Rate* $P_{\text{success}}(d)$: To a given distance d , the transmittance (6) and the initial fidelity (34) are the fixed numbers, so we can determine whether the initial fidelity qualifies by comparing it with the fidelity threshold F_{th} :

$$P_{\text{success}}(d) = \begin{cases} 1, & \text{if } F'_0 \geq F_{th} \\ 0, & \text{if } F'_0 < F_{th} \end{cases} \quad (47)$$

If $F'_0 \geq F_{th}$, the link initial fidelity qualifies absolutely, so the probability is 1, otherwise, the link is not qualified with a lower fidelity than the threshold, the probability is 0.

To further analyze this probability, we need to define a maximum transmission distance d_{max} , which is the distance that makes the fidelity exactly equal to the threshold $F'_0(d_{max}) = F_{th}$. Inspired by unit disk graphs (UDG) [42]–[44], due to the farther the distance, the lower the transmittance, the larger impact from the rotation, $F'_0(d)$ is a monotonically decreasing function. Therefore, we can derive the success rate of fidelity qualification with distance as:

$$P_{\text{success}}(d) = \begin{cases} 1, & \text{if } d \leq d_{max} \\ 0, & \text{if } d > d_{max} \end{cases} \quad (48)$$

Now, we need to calculate the maximum transmission distance. According to (6) and (35), $F'_0(t)$ can be a function of d by using $t = \frac{d}{c}$, where d is the distance, and c is the speed of light. Therefore, the maximum transmission distance can be calculated by:

$$\begin{aligned}
F'_0(d_{max}) &= F_{th} \\
(F_{rotation}(d_{max})) \times F'_0(\eta(d_{max})) &= F_{th} \\
\frac{1}{2} \left[1 + \cos \left(\frac{2v_{sat} \cdot d_{max}}{c(RE + h_{sat})} \right) e^{-2\sigma_{rotation}^2} \right] \times \left[\frac{\eta(d_{max}) + (1 - \eta(d_{max})) \cdot \varepsilon}{1 + 3(1 - \eta(d_{max})) \cdot \varepsilon} \right] &= F_{th} \\
\frac{1}{2} \left[1 + \cos \left(\frac{2v_{sat} \cdot d_{max}}{c(RE + h_{sat})} \right) e^{-2\sigma_{rotation}^2} \right] \times \left[\frac{\left(1 - e^{-\frac{2R_{ap}^2}{\theta^2 d_{max}^2}} \right) + \left(1 - \left(1 - e^{-\frac{2R_{ap}^2}{\theta^2 d_{max}^2}} \right) \right) \cdot \varepsilon}{1 + 3 \left(1 - \left(1 - e^{-\frac{2R_{ap}^2}{\theta^2 d_{max}^2}} \right) \right) \cdot \varepsilon} \right] &= F_{th} \\
\frac{1}{2} \left[1 + \cos \left(\frac{2v_{sat} \cdot d_{max}}{c(RE + h_{sat})} \right) e^{-2\sigma_{rotation}^2} \right] \times \frac{1 - (1 - \varepsilon) \cdot e^{-\frac{2R_{ap}^2}{\theta^2 d_{max}^2}}}{1 + 3\varepsilon \cdot e^{-\frac{2R_{ap}^2}{\theta^2 d_{max}^2}}} &= F_{th} \\
\frac{1}{2} \left[1 + \cos \left(\frac{2v_{sat} \cdot d_{max}}{c(RE + h_{sat})} \right) e^{-2\sigma_{rotation}^2} \right] \times \left[1 - (1 - \varepsilon) \cdot e^{-\frac{2R_{ap}^2}{\theta^2 d_{max}^2}} \right] &= F_{th} \cdot \left[1 + 3\varepsilon \cdot e^{-\frac{2R_{ap}^2}{\theta^2 d_{max}^2}} \right]
\end{aligned}$$

Let $A = \cos \left(\frac{2v_{sat} \cdot d_{max}}{c(RE + h_{sat})} \right) \cdot e^{-2\sigma_{rotation}^2}$, $B = e^{-\frac{2R_{ap}^2}{\theta^2 d_{max}^2}}$, then it becomes:

$$\begin{aligned}
\frac{1}{2}(1 + A) \cdot [1 - (1 - \varepsilon) \cdot B] &= F_{th} \cdot (1 + 3\varepsilon \cdot B) \\
1 + A - (1 - \varepsilon) \cdot B - (1 - \varepsilon) \cdot AB &= 2F_{th} + 6\varepsilon B \cdot F_{th} \\
1 - 2F_{th} &= B \cdot (1 - \varepsilon + 6\varepsilon \cdot F_{th}) - A \cdot [1 - (1 - \varepsilon) \cdot B] \\
(1 - 2F_{th}) - \exp \left(-\frac{2R_{ap}^2}{\theta^2 d_{max}^2} \right) \cdot [1 - \varepsilon + 6F_{th}\varepsilon] &= -\cos \left(\frac{2v_{sat} \cdot d_{max}}{c(RE + h_{sat})} \right) \cdot e^{-2\sigma_{rotation}^2} \cdot \left[1 - \exp \left(-\frac{2R_{ap}^2}{\theta^2 d_{max}^2} \right) \cdot (1 - \varepsilon) \right]
\end{aligned} \tag{49}$$

This is a mixed transcendental equation, the index term $\exp \left(-\frac{2R_{ap}^2}{\theta^2 d_{max}^2} \right)$ is from beam diffraction, the triangle term $\cos \left(\frac{2v_{sat} \cdot d_{max}}{c(RE + h_{sat})} \right)$ is from polarization rotation. The cosine and exponential functions are coupled, d_{max} appears both in exponential function (as d_{max}^2) and cosine function (as d_{max}). According to the transcendental equation theory, these types of equations generally do not have closed algebraic solutions. Also, because when the transmission distance is very short (40 – 50km), $e^{-2\sigma_{rotation}^2} \approx 1$, the impact of rotation on fidelity is very small, so it is reasonable to ignore rotation, but only consider QBER and pointing error, to simplify eq. (49) as follows:

$$\begin{aligned}
F_0(d_{max}) &= F_{th} \\
\frac{\eta(d_{max}) + (1 - \eta(d_{max})) \cdot \varepsilon}{1 + 3(1 - \eta(d_{max})) \cdot \varepsilon} &= F_{th} \\
\eta(d_{max}) + (1 - \eta(d_{max})) \cdot \varepsilon &= F_{th} \cdot [1 + 3(1 - \eta(d_{max})) \cdot \varepsilon] \\
\eta(d_{max})[1 - \varepsilon + 3F_{th}\varepsilon] &= F_{th} + 3F_{th}\varepsilon - \varepsilon \\
\eta(d_{max}) &= \frac{F_{th}(1 + 3\varepsilon) - \varepsilon}{1 + \varepsilon(3F_{th} - 1)} \\
1 - \exp \left(-\frac{2\pi^2 W_0^2 R_{ap}^2}{\omega^2 d_{max}^2} \right) &= \frac{F_{th}(1 + 3\varepsilon) - \varepsilon}{1 + \varepsilon(3F_{th} - 1)} \\
\exp \left(-\frac{2\pi^2 W_0^2 R_{ap}^2}{\omega^2 d_{max}^2} \right) &= \frac{1 - F_{th}}{1 + \varepsilon(3F_{th} - 1)} \\
-\frac{2\pi^2 W_0^2 R_{ap}^2}{\omega^2 d_{max}^2} &= \ln \left[\frac{1 - F_{th}}{1 + \varepsilon(3F_{th} - 1)} \right] \\
d_{max}^2 &= -\frac{2\pi^2 W_0^2 R_{ap}^2}{\omega^2 \ln \left[\frac{1 - F_{th}}{1 + \varepsilon(3F_{th} - 1)} \right]} \\
d_{max} &= \sqrt{\frac{-2R_{ap}^2}{\theta^2 \ln \left[\frac{1 - F_{th}}{1 + \varepsilon(3F_{th} - 1)} \right]}}
\end{aligned} \tag{50}$$

For making d_{max} to be a meaningful positive real number, the following requirements need to be satisfied:

- 1) The logarithmic argument must be positive:

$$\frac{1 - F_{th}}{1 + \varepsilon(3F_{th} - 1)} > 0 \quad (51)$$

Due to $F_{th} \in (0, 1) \Rightarrow 1 - F_{th} > 0$, so:

$$\begin{aligned} 1 + \varepsilon(3F_{th} - 1) &> 0 \\ \varepsilon(3F_{th} - 1) &> -1 \end{aligned} \quad (52)$$

- 2) The radical sign must contain positive values, due to the numerator $-2R_{ap}^2 < 0$, the denominator has to be negative as well, which means:

$$\begin{aligned} \ln \left[\frac{1 - F_{th}}{1 + \varepsilon(3F_{th} - 1)} \right] &< 0 \\ \frac{1 - F_{th}}{1 + \varepsilon(3F_{th} - 1)} &< 1 \\ 1 - F_{th} &< 1 - \varepsilon(1 - 3F_{th}) \\ \varepsilon(1 - 3F_{th}) &> F_{th} \end{aligned} \quad (53)$$

- 3) The basic constraints of physical parameters:

$$\varepsilon \geq 0, R_{ap} > 0, \theta > 0 \quad (54)$$

Now, according to Eq. (52) and (53), we need to consider two conditions:

- 1) $F_{th} \in [\frac{1}{3}, 1) \Rightarrow 3F_{th} - 1 \geq 0$, therefore, in Eq. (51), numerator $1 - F_{th} > 0$, denominator $1 + \varepsilon(3F_{th} - 1) > 0$, so the first requirement is satisfied in this condition. To the second requirement, from Eq. (53), due to $F_{th} \geq \frac{1}{3} \Rightarrow 1 - 3F_{th} \leq 0$, so $\varepsilon(1 - 3F_{th}) \leq 0 < F_{th}$, so the second requirement is satisfied in this condition. As a conclusion, when $F_{th} \in [\frac{1}{3}, 1)$ and $\varepsilon \geq 0$, $d_{max} > 0$ exists.
- 2) $F_{th} \in (0, \frac{1}{3}) \Rightarrow 3F_{th} - 1 < 0$, for the first requirement, from eq. (52), we can derive it as:

$$\varepsilon < -\frac{1}{3F_{th} - 1} = \frac{1}{1 - 3F_{th}} \quad (55)$$

which is the harder requirement of ε .

For the second requirement, from eq. (53), we can derive it as:

$$\begin{aligned} F_{th} &> \varepsilon(1 - 3F_{th}) \\ \varepsilon &< \frac{F_{th}}{1 - 3F_{th}} \end{aligned} \quad (56)$$

For $F_{th} < 1$, $\frac{F_{th}}{1 - 3F_{th}} < \frac{1}{1 - 3F_{th}}$, so the second requirement is more restrictive, therefore, when $F_{th} \in (0, \frac{1}{3})$, ε needs to be $\in [0, \frac{F_{th}}{1 - 3F_{th}})$.

C. Transition Probabilities

1) *Transit from state $(0, d_{odd})$* : When there is no link currently, the system must attempt to generate a new link to satisfy the possible request. Therefore, Node s^t generates an EPR pair with probability p to success, and sends one qubit to the Node \mathfrak{d}^t automatically, cost $t_{trans}(d_{new})$ transition time.

Then, the telescope of Node \mathfrak{d}^t will capture the qubit with probability $q(d_{new})$ with success. Meanwhile, the system can get the transmittance η by the radius of the telescope R_{ap} , the beam waist radius at the transmitter W_0 , and the wavelength of the light through Eq. (6). After that, the system can calculate the initial fidelity F'_0 after the whole link is set up, and determine whether $F'_0 \geq F_{th}$? If yes, then the link is qualified and can be stored in quantum memory, the system transitions to state $(1, d_{new})$. If not, the link is unqualified and should be discarded, the system remains in state $(0, d_{new})$. The transition probability of this system at this condition can be written as:

$$\begin{aligned} P_{(0, d_{old}) \rightarrow (1, d_{new})} &= p \cdot q(d_{new}) \cdot P_{\text{success}}(d_{new}) \\ P_{(0, d_{old}) \rightarrow (0, d_{new})} &= 1 - p \cdot q(d_{new}) \cdot P_{\text{success}}(d_{new}) \\ P_{(0, d_{old}) \rightarrow (j, d_{new})} &= 0, \quad \forall j \geq 2 \end{aligned} \quad (57)$$

2) *Transit from state (i_{store}, d_{odd})* : When there is an available link with age i_{store} and length d_{odd} , its fidelity should be as the Eq. (40) and should higher than the minimum acceptable threshold:

$$F_{current} = \frac{1 + (2F'_0 - 1)e^{-4\Gamma \cdot i_{store} \cdot \Delta t}}{2} \geq F_{th} \quad (58)$$

because if $F_{current} \leq F_{th}$, the link should be useless and discarded, and would not stay at state i_{store} . Then, this link will be consumed to satisfy the request, and the system should try to generate a new link with distance d_{new} for the future request, and so, the system will transit to state $(0, d_{odd})$.

The transition probability of this system at this condition can be written as:

$$\begin{aligned} P_{(i_{store}, d_{old}) \rightarrow (1, d_{new})} &= p \cdot q(d_{new}) \cdot P_{\text{success}}(d_{new}) \\ P_{(i_{store}, d_{old}) \rightarrow (0, d_{new})} &= 1 - p \cdot q(d_{new}) \cdot P_{\text{success}}(d_{new}) \\ P_{(i_{store}, d_{old}) \rightarrow (j, d_{new})} &= 0, \quad \forall j \geq 2 \end{aligned} \quad (59)$$

3) *Transit from the state without request*: If there is no request at a time slot with probability $1 - \lambda$, the system will transit according to the condition whether there is an available link. If there is a link with $i_{store} \geq 1$, then the transition probabilities will be:

$$\begin{aligned} P_{(i_{store}, d) \rightarrow (i_{store} + 1, d)} &= 1, \quad i_{store} < K(d) \\ P_{(K(d), d) \rightarrow (0, d)} &= 1, \quad i_{store} \geq K(d) \end{aligned} \quad (60)$$

If the time the link is stored in memory is still within the maximum storage time, then this link will remain in memory, and the system state will change to $(i_{store} + 1, d)$. If the time the link is stored in memory exceeds the maximum storage time, the link will be discarded at the next moment, and the system state will transit to $(0, d)$, which means there is no available link. If there is no available link ($i_{store} = 0$), the transition probability of this system will remain the same in $(0, d)$ as:

$$P_{(0, d) \rightarrow (0, d)} = 1 \quad (61)$$

D. Performance Metrics

Now we analyze the performance of the Markov chain model with decoherence in the free-space channel and quantum memory, considering $K(d)$ as the maximum age.

1) *Request Satisfaction Rate*: At time t , the system is at state $(i_{store}, d_j) \in S$, where $i_{store} \in \{0, 1, 2, \dots, K(d_j)\}$ is the link storing age in time slot, $d_j \in \mathcal{D}$ is the physical distance of that link. For example, state $(0, d_j)$ presents no available link, the distance of the most recent request is d_j , state $(i_{store}, d_j), i_{store} \geq 1$ presents there is an usable link with age i_{store} time slots and distance d_j . Meanwhile, the state distribution of this system is represented by a probability vector as:

$$\mathbf{P}(t; \lambda) = [P_{(0, d_1)}(t; \lambda), P_{(1, d_1)}(t; \lambda), \dots, P_{(K(d_1), d_1)}(t; \lambda), P_{(0, d_2)}(t; \lambda), \dots] \quad (62)$$

$$\mathbf{P}(t+1) = \mathbf{P}(t) \cdot \mathcal{T}(\lambda) \quad (63)$$

It consists of one request with distance d_1 followed by another with distance d_2 and another \dots . And it should satisfy normalization conditions:

$$\sum_{d_j \in \mathcal{D}} \sum_{i=0}^{K(d_j)} P_{(i, d_j)}(t) = 1 \quad (64)$$

Here, we want to calculate the probability that an incoming request with distance d_{new} is successfully satisfied $R(t)$, at time t . According to the law of total probability, the request fulfillment rate can be expressed as:

$$R(t) = \sum_{s \in S} P(s, t) \cdot P(\text{request satisfied} \mid \text{current status} = s) \quad (65)$$

where $P(s, t)$ is the probability of the system be at state s at time t .

A request arriving can be satisfied in two ways:

Case 1: Using an existing link When the system is in state (i_{store}, d_j) with $i_{store} \geq 1$, there is an available link with age i_{store} time slots, fidelity $F(i_{store}) = \frac{1+2F_0'(t-1) \cdot e^{-4\Gamma \cdot i_{store} \cdot \Delta t}}{2} \geq F_{th}$. Since the link exists and its fidelity meets the requirements (otherwise it would have been discarded long ago), this link can be used immediately to fulfill the request. Therefore, the probability of this condition being met is:

$$P(\text{request satisfied} \mid \text{state} = (i_{store}, d_j), i_{store} \geq 1) = 1 \quad (66)$$

Case 2: Generating a new link When the system is in state $(0, d_j)$, there is no available link currently, the system must try to generate a new link with distance d_{new} , which needs the success of all three processes:

- 1) EPR pair successfully generated: probability p ;
- 2) Photon transmission successful: probability $q(d_{new})$;
- 3) Fidelity qualified: probability $P_{success}(d_{new})$

We define the overall success rate of them as $p' = p \cdot q(d_{new}) \cdot P_{success}(d_{new})$, and the probability of this condition being met is $P(\text{request satisfied} \mid \text{state} = (0, d_j), d_{new}) = p'(d_{new})$.

Therefore, the rate of a request being satisfied at each time slot should be the sum of the probabilities of Case 1 and Case 2 with λ :

$$\begin{aligned} R(t, d_{new}; \lambda) &= \sum_{d_j \in \mathcal{D}} \sum_{i=1}^{K(d_j)} P_{(i, d_j)}(t; \lambda) \cdot P(\text{request satisfied} \mid (i, d_j)) \\ &\quad + \sum_{d_j \in \mathcal{D}} P_{(0, d_j)}(t; \lambda) \cdot P(\text{request satisfied} \mid (0, d_j), d_{new}) \\ &= \sum_{d_j \in \mathcal{D}} \sum_{i=1}^{K(d_j)} P_{(i, d_j)}(t; \lambda) \cdot 1 + \sum_{d_j \in \mathcal{D}} P_{(0, d_j)}(t; \lambda) \cdot p'(d_{new}) \\ &= \left[1 - \sum_{d_j \in \mathcal{D}} P_{(0, d_j)}(t; \lambda) \right] + \sum_{d_j \in \mathcal{D}} P_{(0, d_j)}(t; \lambda) \cdot p'(d_{new}) \\ &= 1 - \sum_{d_j \in \mathcal{D}} P_{(0, d_j)}(t; \lambda) \cdot [1 - p'(d_{new})] \end{aligned} \quad (67)$$

Here, to simplify this equation, define the total no-link probability as:

$$\begin{aligned} P_0(t; \lambda) &:= \sum_{d_j \in \mathcal{D}} P_{(0, d_j)}(t; \lambda) \\ &:= \sum_{d_j \in \mathcal{D}} [\mathbf{P}(0) \cdot \mathcal{T}(\lambda)^t]_{(0, d_j)} \\ &:= \sum_{d_j \in \mathcal{D}} [\mathbf{P}(0) \cdot [\lambda \mathcal{T}_{d_{new}} + (1 - \lambda) \mathcal{T}_{d_j}]^t]_{(0, d_j)} \end{aligned} \quad (68)$$

Then the satisfaction rate simplifies to:

$$R(t, d_{new}; \lambda) = 1 - P_0(t; \lambda) \cdot [1 - p'(d_{new})] \quad (69)$$

Therefore, the satisfaction rate depends on λ through $P_0(t; \lambda)$, which represents the probability of having no available link at time t . Higher λ leads to faster link consumption, increasing $P_0(t; \lambda)$ and potentially decreasing the satisfaction rate. And the average rate of the requests being satisfied in a time window $[0, T]$ is:

$$\begin{aligned} \bar{R}(T, d_{new}; \lambda) &= \frac{1}{T} \sum_{t=1}^T R(t, d_{new}; \lambda) \\ &= \frac{1}{T} \sum_{t=1}^T [1 - P_0(t; \lambda) \cdot [1 - p'(d_{new})]] \\ &= 1 - [1 - p'(d_{new})] \cdot \frac{1}{T} \sum_{t=1}^T P_0(t; \lambda) \end{aligned} \quad (70)$$

2) *Average Waiting Time*: We define the average waiting time $\mathbb{E}[W]$ as the expected number of time slots a request must wait before being satisfied. When a request arrives at the system, there are two cases:

Case 1: Link available The state is in $(i_{store}, d_j), i \in [1, K(d_j)]$, the waiting time is $W = 0$, the request has been satisfied immediately.

Case 2: No link available The state is $(0, d_j)$, so the request must wait for successful link generation, and the number of

attempts until success follows a geometric distribution [21], the probability of success at the attempt k is $(1 - p')^{k-1} \cdot p'$. If the first attempt succeeds with probability p' , then the total number of attempts needed is 1, which contributes to the expectation as $1 \cdot p'$. If the first attempt fails with probability $1 - p'$, then the system wasted 1 attempt already, and assume it still needs to expect E more attempts until reaching the memory capacity threshold. Therefore, it needs $1 + E$ attempts in total, which contributes to expectation with $(1 + E) \cdot (1 - p')$. By the law of total expectation, we have:

$$\begin{aligned} E &= 1 \cdot p' + (1 + E) \cdot (1 - p') \\ E &= p' + (1 - p') + (1 - p') \cdot E \\ E - (1 - p') \cdot E &= 1 \\ E \cdot p' &= 1 \\ E &= \frac{1}{p'} \end{aligned} \quad (71)$$

Assume each generation attempt takes Δt time slots, the expected waiting time from state $(0, d_j)$ is:

$$\mathbb{E}[W \mid \text{state} = 0] = E \cdot \Delta t = \frac{\Delta t}{p'} \text{ time slots} \quad (72)$$

Using the law of total expectation, we have:

$$\begin{aligned} \mathbb{E}[W] &= P_{(0, d_j)} \cdot \mathbb{E}[W \mid (0, d_j)] \\ &+ P_{(i_{store}, d_j)} \cdot \mathbb{E}[W \mid (i_{store}, d_j)] \\ &= P_{(0, d_j)} \cdot \frac{\Delta t}{p'} + P_{(i_{store}, d_j)} \cdot 0 \\ &= P_{(0, d_j)} \cdot \frac{\Delta t}{p'} \end{aligned} \quad (73)$$

Now, we need to determine $P_{(0, d_j)}$. From any state, after consuming, the system has to attempt to generate a new link, which has probability p' to generate successfully, and transition to state $P_{(1, d_j)}$, or has probability $1 - p'$ to generate failure, and stay in state $P_{(0, d_j)}$.

Therefore, for the general case with request arrival rate λ , $P_{(0, d_j)}$ should be obtained from the steady state distribution of the Markov chain defined in Eq. (68) as:

$$P_{(0, d_j)}(\infty; \lambda) = \lim_{t \rightarrow \infty} \sum_{d \in \mathcal{D}} P_{(0, d_j)}(t; \lambda) \quad (74)$$

Therefore, the general average waiting time is:

$$\mathbb{E}[W \mid \lambda] = P_{(0, d_j)}(\infty; \lambda) \cdot \frac{\Delta t}{p'} \quad (75)$$

And for the special case $\lambda = 1$, when a request arrives at every time slot, after each request is handled, the probability of being in state $(0, d_j)$ is $P_{(0, d_j)}(\infty; 1) = 1 - p'$. Therefore, the expected waiting time is:

$$\begin{aligned} \mathbb{E}[W \mid \lambda = 1] &= P_{(0, d_j)}(\infty; \lambda = 1) \cdot \frac{\Delta t}{p'} \\ &= (1 - p') \cdot \frac{\Delta t}{p'} = \Delta t \left(\frac{1}{p'} - 1 \right) \end{aligned} \quad (76)$$

3) *Link Utilization Efficiency*: Link utilization efficiency measures the fraction of generated entanglement links that are consumed to satisfy requests, rather than expiring due to timeout. Consider a variable request arrival rate $\lambda \in [0, 1]$, where λ is the probability that a request arrives in any given time slot. This system's dynamics change based on whether a request arrives:

Case 1: If request arrives (probability λ) If the system is in state $(i_{store}, d_j), i \geq 1$, the existing link is consumed to satisfy the request. If the system is in state $(0, d_j)$, then try to generate a new entanglement link with distance d_{new} .

Case 2: If no request arrives (probability $1 - \lambda$) The existed link aged by 1 time slot, the system will transition from state (i_{store}, d_j) to state $(i_{store} + 1, d_j)$ if $i_{store} < K(d_j)$, or the link would expire if $i_{store} = K(d_j)$.

For a link generated at time t , we then analyze its possible outcomes over the next $K(d_j)$ time slots. If no request arrives for the first $k - 1$ time slots with probability $(1 - \lambda)^{k-1}$, and a request arrives at the k -th time slot with probability λ , this link will be consumed at age $k \in [1, K(d_j)]$ with probability:

$$P(\text{consumed at age } k) = \lambda(1 - \lambda)^{k-1}, 1 \leq k \leq K(d_j) \quad (77)$$

And the probability a link expires when no request arrives for $K(d_j)$ consecutive time slots is:

$$P_{expire} = (1 - \lambda)^{K(d_j)} \quad (78)$$

Therefore, the link utilization efficiency $\Xi(\lambda)$ is:

$$\begin{aligned} \Xi(\lambda) &= \sum_{k=1}^{K(d_j)} P(\text{consumed at age } k) = \sum_{k=1}^{K(d_j)} \lambda(1 - \lambda)^{k-1} \\ &= \lambda \cdot \frac{1 - (1 - \lambda)^{K(d_j)}}{1 - (1 - \lambda)} = \lambda \cdot \frac{1 - (1 - \lambda)^{K(d_j)}}{\lambda} \\ &= 1 - (1 - \lambda)^{K(d_j)} \end{aligned} \quad (79)$$

Therefore, theoretically, when there is a high request rate ($\lambda \rightarrow 1$), nearly all links can be consumed ($\Xi \rightarrow 1$). When there is a low request rate ($\lambda \rightarrow 0$), nearly all links would be discarded ($\Xi \rightarrow 0$). And when no limitation to the cutoff time ($K(d_j) \rightarrow \infty$), all links can be consumed ($\Xi \rightarrow 1$) for any request rate of $\lambda > 0$.

4) *Average Link Fidelity of Consumption*: According to Eq. (40), we can get the average link fidelity of consumption by calculating the average link age of consumption. When a request arrives and the system is in state $(i_{store}, d_j), i \in [1, K(d_j)]$, it consumes a link of age $i_{store} \cdot \Delta t$. The probability distribution over states $(i_{store}, d_j), i \in [2, K(d_j)]$ depends on the request arrival rate λ . Generally, a link generated at time t (the system entering to state $(1, d_j)$) is consumed at age $k \in \{1, 2, \dots, K(d_j)\}$ if there was no request arrives for $k - 1$ time slots, with probability of $(1 - \lambda)^{k-1}$, and a request arrives at the k -th time slot with probability λ . Therefore, considering the conditional probability and Bayes' Theorem with Eq. (77),

Eq. (78) and Eq. (79), the probability of a link being consumed at age k is:

$$\begin{aligned} P(\text{age} = k \mid \text{consumed}) &= \frac{P(\text{age} = k \text{ and consumed})}{P(\text{consumed})} \\ &= \frac{P(\text{age} = k \text{ and consumed})}{1 - P_{\text{expire}}} \quad (80) \\ &= \frac{\lambda(1 - \lambda)^{k-1}}{1 - (1 - \lambda)^{K(d_j)}} \end{aligned}$$

Therefore, the expected age right at consumption in the time slot should be:

$$\begin{aligned} \mathbb{E}[\text{age at consumption (slots)}] &= \sum_{k=1}^{K(d_j)} k \cdot P(\text{age} = k \mid \text{consumed}) \\ &= \frac{\lambda}{1 - (1 - \lambda)^{K(d_j)}} \sum_{k=1}^{K(d_j)} k(1 - \lambda)^{k-1} \quad (81) \end{aligned}$$

And the expected age at consumption in time units should be:

$$\begin{aligned} \mathbb{E}[\text{age at consumption}] &= \Delta t \cdot \mathbb{E}[\text{age at consumption (slots)}] \\ &= \frac{\lambda \Delta t}{1 - (1 - \lambda)^{K(d_j)}} \sum_{k=1}^{K(d_j)} k(1 - \lambda)^{k-1} \quad (82) \end{aligned}$$

Specifically, when requests arrive at every time slot ($\lambda = 1$), all links are consumed at age 1, and so the average link age at consumption is:

$$\mathbb{E}[\text{age at consumption} \mid \lambda = 1] = \Delta t \quad (83)$$

Therefore, theoretically, if the system faces a high request rate ($\lambda \rightarrow 1$), the links would be consumed quickly ($\mathbb{E}[\text{age}] \rightarrow \Delta t$). If the request rate is low ($\lambda \rightarrow 0$), among the consumed links, they are tend to wait longer before consumption, as $\mathbb{E}[\text{age} \mid \text{consumed}] \rightarrow \frac{(K(d_j)+1)\Delta t}{2}$, which is the uniform distribution over $[1, K(d_j)]$. Also, if the entangled states can be stored for infinite time ($K(d_j) \rightarrow \infty$), $\mathbb{E}[\text{age} \mid \text{consumed}] \rightarrow \frac{\Delta t}{\lambda}$ for fixed $\lambda > 0$.

This metric reveals the trade-off between memory occupancy and latency, where a smaller $\mathbb{E}[\text{age at consumption}]$ means links are used quickly, with low memory pressure and low latency. And larger $\mathbb{E}[\text{age at consumption}]$ indicates links wait longer in memory, facing higher decoherence, potentially lower fidelity at use. We now calculate the expected fidelity of links when they are actually used. According to Eq. (40) and the conditional probability from Eq. (80), the expected fidelity

of a consumed link is:

$$\begin{aligned} \mathbb{E}[F_{\text{consumed}}] &= \sum_{k=1}^{K(d_j)} F(k) \cdot P(\text{age} = k \mid \text{consumed}) \\ &= \sum_{k=1}^{K(d_j)} F'_0 \cdot e^{-2\Gamma \cdot t_{\text{store}}} \cdot \frac{\lambda(1 - \lambda)^{k-1}}{1 - (1 - \lambda)^{K(d_j)}} \\ &= F'_0 \cdot \frac{\lambda}{1 - (1 - \lambda)^{K(d_j)}} \cdot \sum_{k=1}^{K(d_j)} e^{-2\Gamma \cdot k \cdot \Delta t} \cdot (1 - \lambda)^{k-1} \\ &= F'_0 \cdot \frac{\lambda}{1 - (1 - \lambda)^{K(d_j)}} \cdot \sum_{k=1}^{K(d_j)} [(1 - \lambda) \cdot e^{-2\Gamma \cdot \Delta t}]^{k-1} \cdot e^{-2\Gamma \cdot \Delta t} \quad (84) \end{aligned}$$

Let $\iota = (1 - \lambda)e^{-2\Gamma \Delta t}$, then the geometric series gives $\sum_{k=1}^{K(d_j)} \iota^{k-1} e^{-2\Gamma \Delta t} = e^{-2\Gamma \Delta t} \cdot \frac{1 - \iota^{K(d_j)}}{1 - \iota}$, therefore:

$$\mathbb{E}[F_{\text{consumed}}] = F'_0 \cdot e^{-2\Gamma \Delta t} \cdot \frac{\lambda \cdot (1 - \iota^{K(d_j)})}{(1 - (1 - \lambda)^{K(d_j)})(1 - \iota)} \quad (85)$$

where $\iota = (1 - \lambda)e^{-2\Gamma \Delta t}$.

Therefore, theoretically, if there is a request at each time slot ($\lambda = 1$), all links will be consumed at age 1, so $\mathbb{E}[F_{\text{consumed}} \mid \lambda = 1] = F(1) = F'_0 \cdot e^{-2\Gamma \Delta t}$. If there is a low request rate ($\lambda \rightarrow 0$), the consumed links tend to be older, as they have to wait longer for a request, so the expected fidelity of this condition over all possible ages of $[1, K(d_j)]$ is:

$$\begin{aligned} \lim_{\lambda \rightarrow 0} \mathbb{E}[F_{\text{consumed}}] &= \frac{1}{K(d_j)} \sum_{k=1}^{K(d_j)} F(k) \\ &= \frac{1}{K(d_j)} \sum_{k=1}^{K(d_j)} F'_0 \cdot e^{-2\Gamma \cdot k \cdot \Delta t} \quad (86) \\ &= \frac{F'_0}{K(d_j)} \cdot \sum_{k=1}^{K(d_j)} e^{-2\Gamma \cdot k \cdot \Delta t} \end{aligned}$$

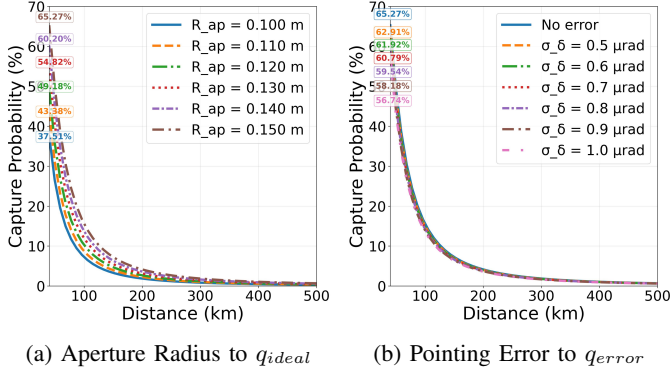
In summary, we can observe that there is a trade-off between request satisfaction rate and link fidelity. Theoretically, higher λ causes links to be consumed faster, with higher fidelity, but potentially lowers the satisfaction rate if the generation processes are slow. Lower λ causes links to wait longer, so they would be used with lower fidelity, but the system can have a higher probability of having available links.

IV. EVALUATION

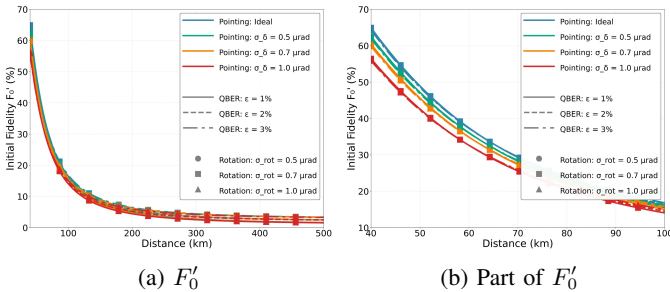
This section presents the evaluation of this one-hop Markov chain model. It shows the trends in capture probability, initial fidelity, and fidelity of an EPR pair stored in quantum memories. Also, this section provides the cutoff time and the maximum transmission distance for a single hop. Table II shows the values of all the symbols that will be used in our evaluation process, all values of parameters have their references. Among them, $F_{th} \geq 0.5$ is the minimum request of fidelity that can be purified to get higher fidelity [45].

TABLE II: Parameters of Evaluation

Symbol	Value	Facility / Note
θ	$5 \mu\text{rad}$	Micius [3], [25], Jinan-1 [46]
R_{ap}	100–150 mm	Micius [3], Jinan-1 [46]
σ_δ	0.5–1.0 μrad	Micius [47]
ε	1%–3%	Micius [48]
Γ	$0.5\text{--}1 \text{ s}^{-1}$	Trapped ion [49]
F_{th}	0.5	Min. F_{purify} [45]
d	40–150 km	Starlink [9]
v_{sat}	7.589 km/s	Starlink [9]
h_{sat}	550 km	Starlink [9]
$\sigma_{rotation}$	$< 1 \mu\text{rad}$	GOES-16 [50]


 Fig. 3: Capture Probability (q)

The figure 3(a) shows the trend of q_{ideal} of different conditions of the aperture radius under the ideal circumstance, that is, without the pointing error. In this figure, the larger the aperture, the higher the q_{ideal} , with a maximum value of 65.27% when the transmission distance is 40km. The figure 3(b) shows the trend of q_{error} of different pointing errors with the aperture radius of 0.15m on the satellite. In this figure, the lower the pointing error, the higher the q_{error} . Although this figure shows not many differences between all conditions, q_{error} still varies from 62.91% to 56.74% at 40km, as the pointing errors are larger. Also, in both figures of Fig. 3, all q drops very quickly when the distance is 40 – 100km, which shows the maximum distance should be lower than 100km.


 Fig. 4: Initial Fidelity (F'_0)

The figure 4 shows the trend in initial fidelity of an EPR pair, after the single photon is captured successfully by satellite B. Although theoretically, the flying distance range of LEO

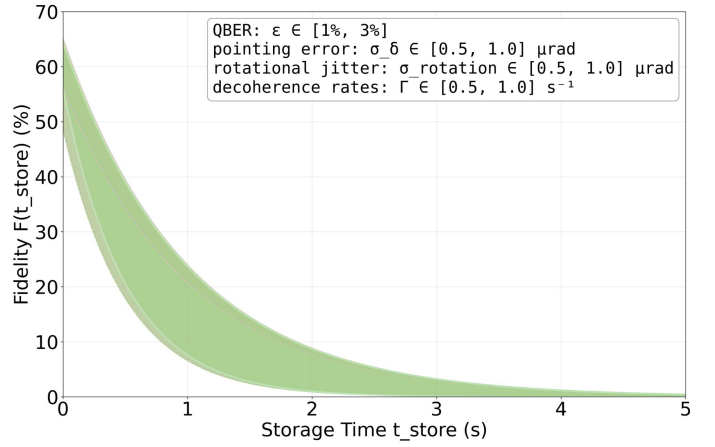


Fig. 5: Fidelity Evolution Range

satellite is 200 – 2000km above the Earth, the results in Fig. 4(a) show F'_0 drops very quickly before 100km, so the transmission distance of one-hop is very limited. Therefore, we analyze the typical distance range of 40 – 100km, as Fig. 4(b) shows. With different kinds of errors, F'_0 varies from 64.95% to 55.86% at 40km, varies from 57.57% to 49.58% at 44.24km. Therefore, we will analyze within the distance range of 40km to 45km.

The green region in Fig. 5 shows the fidelity evolution range for a specific combination of QBER $\varepsilon \in [1\%, 3\%]$, pointing error $\sigma_\delta \in [0.5, 1.0] \mu\text{rad}$ and rotational jitter $\sigma_{rotation} \in [0.5, 1.0] \mu\text{rad}$, spanning all satellite distances $d \in [40, 45] \text{ km}$ and decoherence rates $\Gamma \in [0.5, 1.0] \text{ s}^{-1}$. From this figure, we can observe that under the severe satellite environment, the fidelity of the EPR pair stored in quantum memories is decreasing very quickly, even can not even last for 0.5s, because $F_{store} < 50\%$ when $t_{store} > 0.5 \text{ s}$. Therefore, the cutoff time of the LEO satellite environment must be shorter than 0.5s.

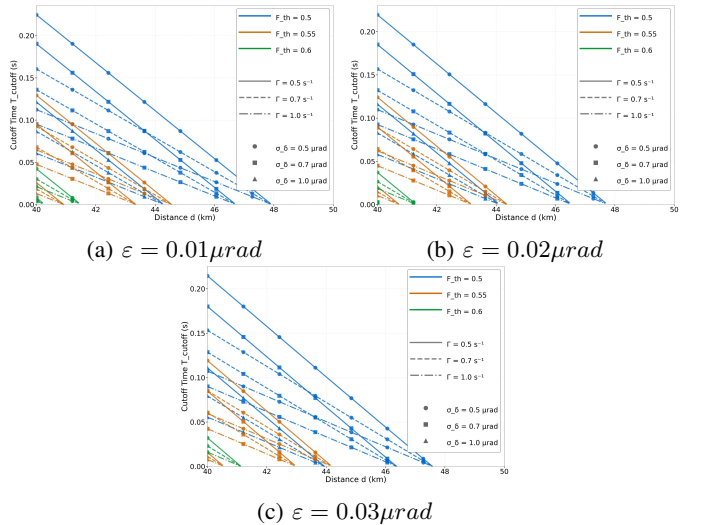


Fig. 6: Cutoff Time

The Fig. 6 shows the linear relationship of cutoff time to the transmission distance, the orbital height is 550 km, and the velocity of the satellite is 7.589 km/s. Due to $e^{-2\sigma_{rotation}} \approx 1$ when the transmission distance is short, the polarization rotation has very little impact on the cutoff time, so we set $\sigma_{rotation} = 0.7\mu rad$ in this figure. We can see that all T_{cutoff} tends to decrease as the distance becomes longer, F_{th} becomes smaller, Γ becomes larger, and σ_{δ} becomes larger. When $\varepsilon = 0.01\mu rad$, the maximum $T_{cutoff} = 0.224s$, with $F_{th} = 0.5, \Gamma = 0.5s^{-1}, \sigma_{\delta} = 0.5\mu rad$ at $40km$. When $\varepsilon = 0.02\mu rad$, the maximum T_{cutoff} reduces to $0.219s$, and it is $0.214s$ when $\varepsilon = 0.03\mu rad$.

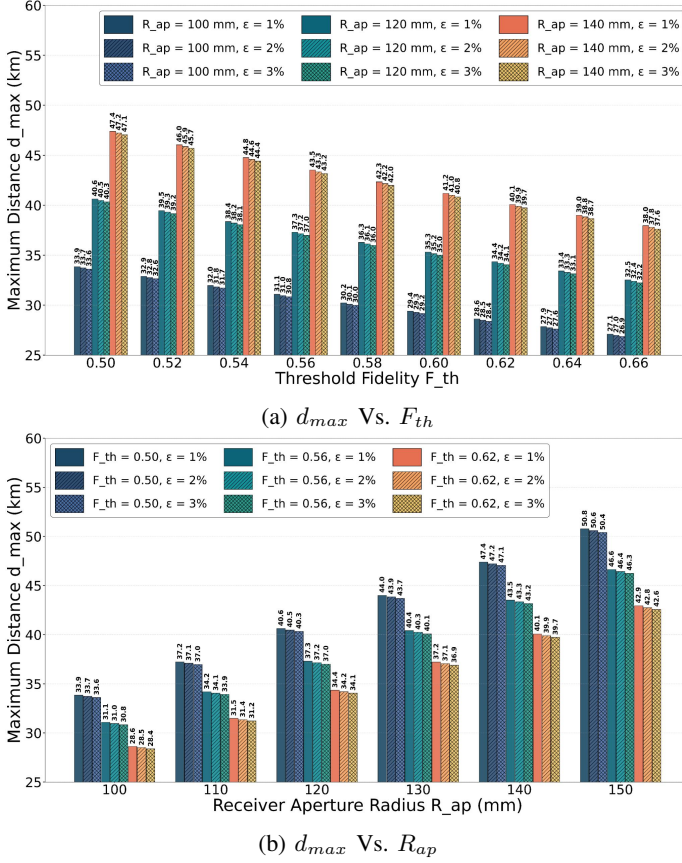


Fig. 7: Maximum Transmission Distance d_{max}

Fig. 7 shows the maximum one-hop transmission distance under different requirements, with a QBER range of $[1, 3]\%$, but without polarization rotation. Here, d_{max} is increasing with larger R_{ap} , but decreasing with higher ε and F_{th} . However, the minimum d_{max} requirement of Starlink is $40km$, so the maximum $F_{th} = 0.62$ through the observation of Fig. 7(a). Therefore, the fidelity range of Fig. 7(b) is $[0.5, 0.62]$. In this figure, the maximum d_{max} is $50.78km$, with $F_{th} = 0.5, \varepsilon = 1\%$, and $R_{ap} = 150mm$, but without polarization rotation. Also, the minimum allowable aperture radius should be $120mm$ with $F_{th} = 0.5$, because all the more severe cases have the $d_{max} < 40km$. Through the far right results of Fig. 7(b), all $d_{max} > 40km$, so we encourage equipping

telescopes on satellites with $R_{ap} \geq 150mm$.

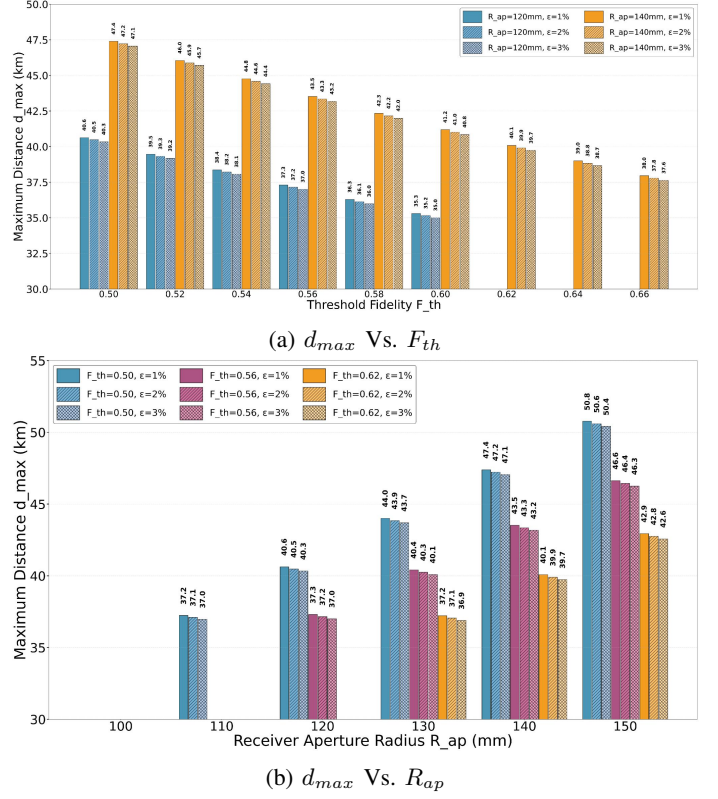


Fig. 8: Maximum Transmission Distance d_{max} with Rotation

Then, Fig. 8 shows the results of d_{max} with $\sigma_{rotation} = 0.7\mu rad$. The trend is similar to Fig. 7, the highest $d_{max} = 50.776952km$ when $F_{th} = 0.5, \varepsilon = 1\%$. It is noticed that with polarization rotation, the initial fidelity F_0' decreases lower than the threshold, so $p' = 0$ under these tough conditions, and it needs larger receiving equipment to overcome this issue, which is why there is no result in Fig. 8(b) when $R_{ap} = 100mm$. Moreover, table III has the clear comparison of d_{max} with or without $\sigma_{rotation}$. These results show polarization has little impact on d_{max} , if $p' = 1$ and there is available d_{max} , therefore, it is reasonable to ignore polarization rotation while analyzing the maximum one-hop transmission distance within $40 - 50km$.

TABLE III: d_{max} Comparison

ε	Mean Diff. (km)	Max Diff. (km)	Relative Diff. (%)
1%	5.3×10^{-9}	2.48×10^{-7}	1.06×10^{-7}
2%	2.07×10^{-8}	2.41×10^{-7}	1.12×10^{-7}
3%	1.11×10^{-8}	2.31×10^{-7}	1.09×10^{-7}

V. CONCLUSION

As conclusion, this paper presents the first comprehensive Markov chain model specifically designed for analyzing entanglement distribution in dynamic LEO satellite quantum networks operating in a noisy free-space environment.

By introducing a novel two-dimensional state space that simultaneously captures physical distance and storage age, our model accurately characterizes the unique challenges of satellite-based quantum communication, including geometric beam divergence, pointing errors, polarization rotation, and quantum memory decoherence. Moreover, we derive analytical expressions for four critical performance metrics, which are request satisfaction rate, average waiting time, link utilization efficiency, and average consumed link fidelity, that reveal the fundamental tradeoffs inherent to satellite quantum networks. Our analysis demonstrates that higher request arrival rates lead to faster link consumption with higher fidelity but potentially lower satisfaction rates, because it may be hard to generate new links when ρ' is small. Lower request rates can result in longer storage times at the cost of reduced fidelity due to increased decoherence effects.

Also, the evaluation results provide guidelines for satellite quantum communication systems. We establish that the maximum one-hop transmission distance is limited to approximately 40–50 km under realistic error conditions, with cutoff time constrained to below 0.3 s in harsh satellite environments. Importantly, we prove that polarization rotation effects can be reasonably neglected for short transmission distances (40–50 km), simplifying system analysis and design. These findings provide crucial theoretical foundations for developing efficient entanglement routing algorithms and optimizing resource allocation strategies in practical satellite quantum networks.

We know the drawback of this model is that it may cause qubit resource wastage due to we pre-generate the link and wait for the request, but the wastage is not that severe in our two-node system. Therefore, we will extend this model to an on-demand link generation strategy with multi-hop scenarios to reduce the qubit resource further. In summary, this novel model enables comprehensive performance analysis of global-scale quantum communication networks and supports the development of practical quantum internet infrastructure.

REFERENCES

- [1] M. Pittaluga, M. Minder, M. Lucamarini, M. Sanzaro, R. I. Woodward, M.-J. Li, Z. Yuan, and A. J. Shields, “600-km Repeater-Like Quantum Communications With Dual-Band Stabilization,” *Nature Photonics*, vol. 15, no. 7, pp. 530–535, 2021.
- [2] T. Gonzalez-Raya, S. Pirandola, and M. Sanz, “Satellite-Based Entanglement Distribution and Quantum Teleportation With Continuous Variables,” *Communications Physics*, vol. 7, no. 1, p. 126, 2024.
- [3] S.-K. Liao, W.-Q. Cai, W.-Y. Liu, L. Zhang, Y. Li, J.-G. Ren, J. Yin, Q. Shen, Y. Cao, Z.-P. Li *et al.*, “Satellite-to-Ground Quantum Key Distribution,” *Nature*, vol. 549, no. 7670, pp. 43–47, 2017.
- [4] D. Pan, X.-T. Song, and G.-L. Long, “Free-Space Quantum Secure Direct Communication: Basics, Progress, and Outlook,” *Advanced Devices & Instrumentation*, vol. 4, p. 0004, 2023.
- [5] M. Sisodia, V. Venkataraman, J. Ghosh *et al.*, “FSO-QKD Protocols Under Free-Space Losses and Device Imperfections: A Comparative Study,” *Quantum Information Processing*, vol. 23, no. 5, 2024.
- [6] S.-K. Liao, H.-L. Yong, C. Liu, G.-L. Shentu, D.-D. Li, J. Lin, H. Dai, S.-Q. Zhao, B. Li, J.-Y. Guan *et al.*, “Long-Distance Free-Space Quantum Key Distribution in Daylight Towards Inter-Satellite Communication,” *Nature Photonics*, vol. 11, no. 8, pp. 509–513, 2017.
- [7] J. Meister, P. Kleinpaß, and D. Orsucci, “Simulation of Satellite and Optical Link Dynamics in a Quantum Repeater Constellation,” *EPJ Quantum Technology*, vol. 12, no. 1, p. 5, 2025.
- [8] J.-P. Bourgoin, E. Meyer-Scott, B. L. Higgins, B. Helou, C. Erven, H. Huebel, B. Kumar, D. Hudson, I. D’Souza, R. Girard *et al.*, “A Comprehensive Design and Performance Analysis of Low Earth Orbit Satellite Quantum Communication,” *New Journal of Physics*, vol. 15, no. 2, p. 023006, 2013.
- [9] S. Cakaj, “The Parameters Comparison of the ‘Starlink’ LEO Satellites Constellation for Different Orbital Shells,” *Frontiers in Communications and Networks*, vol. 2, p. 643095, 2021.
- [10] Y. Liao, S. Liu, X. Hong, J. Shi, and L. Cheng, “Integration of Communication and Navigation Technologies Toward LEO-Enabled 6G Networks: A Survey,” *Space: Science & Technology*, vol. 3, p. 0092, 2023.
- [11] M. T. Dabiri, M. Hasna, S. Al-Kuwari, and K. Qaraqe, “Physical Limits of Entanglement-Based Quantum Key Distribution Over Long-Distance Satellite Links,” *arXiv preprint arXiv:2506.20798*, 2025.
- [12] S. Koudia, S. Chatzinotas *et al.*, “Space-Based Quantum Internet: Entanglement Distribution in Time-Varying LEO Constellations,” *arXiv preprint arXiv:2409.17032*, 2024.
- [13] V. D. Tubío, M. Dijkstra, and J. Borregaard, “Satellite-assisted Entanglement Distribution with High-Dimensional Photonic Encoding,” *arXiv preprint arXiv:2505.16751*, 2025.
- [14] M. Gündoğan, J. S. Sidhu, V. Henderson, L. Mazzarella, J. Wolters, D. K. Oi, and M. Krutzik, “Proposal for Space-Borne Quantum Memories for Global Quantum Networking,” *npj Quantum Information*, vol. 7, no. 1, p. 128, 2021.
- [15] L. Billings, “China Shatters ‘Spooky Action at a Distance’ record, Preps for Quantum Internet,” *Scientific American*, vol. 15, 2017.
- [16] A. Zang, J. Chung, R. Kettimuthu, M. Suchara, and T. Zhong, “Analytical Performance Estimations for Quantum Repeater Network Scenarios,” in *2024 International Conference on Quantum Computing and Engineering (QCE)*, vol. 1. IEEE, 2024, pp. 1960–1966.
- [17] E. Shchukin, F. Schmidt, and P. van Loock, “Waiting Time in Quantum Repeaters With Probabilistic Entanglement Swapping,” *Physical Review A*, vol. 100, no. 3, p. 032322, 2019.
- [18] Á. G. Ñesta, G. Vardoyan, L. Scavuzzo, and S. Wehner, “Optimal Entanglement Distribution Policies in Homogeneous Repeater Chains With Cutoffs,” *npj Quantum Information*, vol. 9, no. 1, p. 46, 2023.
- [19] S. Haldar, P. J. Barge, S. Khatri, and H. Lee, “Fast and Reliable Entanglement Distribution With Quantum Repeaters: Principles for Improving Protocols Using Reinforcement Learning,” *Physical Review Applied*, vol. 21, no. 2, p. 024041, 2024.
- [20] W. Dai, A. Rinaldi, and D. Towsley, “The Capacity Region of Entanglement Switching: Stability and Zero Latency,” in *2022 IEEE International Conference on Quantum Computing and Engineering (QCE)*. IEEE, 2022, pp. 389–399.
- [21] Z. Li, H. Gu, X. Wang, and R. Yu, “Dynamic Queuing Analysis and Buffer Management for Entanglement Swapping Buffers with Noise,” in *Proceedings of the 1st Workshop on Quantum Networks and Distributed Quantum Computing*, 2023, pp. 1–6.
- [22] N. K. Panigrahy, T. Vasantam, D. Towsley, and L. Tassiulas, “On the Capacity Region of a Quantum Switch With Entanglement Purification,” in *INFOCOM Conference on Computer Communications*. IEEE, 2023, pp. 1–10.
- [23] S. E. Vinay and P. Kok, “Statistical Analysis of Quantum-Entangled-Network Generation,” *Physical Review A*, vol. 99, no. 4, p. 042313, 2019.
- [24] S. Brand, T. Coopmans, and D. Elkouss, “Efficient Computation of the Waiting Time and Fidelity in Quantum Repeater Chains,” *IEEE Journal on Selected Areas in Communications*, vol. 38, no. 3, pp. 619–639, 2020.
- [25] S.-K. Liao *et al.*, “Satellite-Relayed Intercontinental Quantum Network,” *Physical Review Letters*, vol. 120, no. 3, p. 030501, 2018.
- [26] D. Pan, Z. Lin, J. Wu, H. Zhang, Z. Sun, D. Ruan, L. Yin, and G. L. Long, “Experimental Free-Space Quantum Secure Direct Communication and Its Security Analysis,” *Photonics Research*, vol. 8, no. 9, pp. 1522–1531, 2020.
- [27] E. J. Lee and V. W. Chan, “Part 1: Optical Communication Over the Clear Turbulent Atmospheric Channel Using Diversity,” *IEEE journal on selected areas in communications*, vol. 22, no. 9, pp. 1896–1906, 2004.
- [28] A. Puryear, R. Jin, E. Lee, and V. W. Chan, “Experimental Analysis of the Time Dynamics of Coherent Communication Through Turbulence: Markovianity and Channel Prediction,” in *International Conference on Space Optical Systems and Applications (ICSOS)*. IEEE, 2011, pp. 28–37.

- [29] A. Puryear and V. W. Chan, "On the Time Dynamics of Optical Communication Through Atmospheric Turbulence With Feedback," *Journal of Optical Communications and Networking*, vol. 3, no. 8, pp. 594–609, 2011.
- [30] A. L. Puryear and V. W. Chan, "Optical Communication Through the Turbulent Atmosphere With Transmitter and Receiver Diversity, Wavefront Control, and Coherent Detection," in *Free-Space Laser Communications IX*, vol. 7464. SPIE, 2009, pp. 170–186.
- [31] D. Vasylyev, A. Semenov, and W. Vogel, "Atmospheric Quantum Channels With Weak and Strong Turbulence," *Physical review letters*, vol. 117, no. 9, p. 090501, 2016.
- [32] D. Vasylyev, W. Vogel, and A. Semenov, "Theory of Atmospheric Quantum Channels Based on the Law of Total Probability," *Physical Review A*, vol. 97, no. 6, p. 063852, 2018.
- [33] M. Klen and A. Semenov, "Numerical Simulations of Atmospheric Quantum Channels," *Physical Review A*, vol. 108, no. 3, p. 033718, 2023.
- [34] J. Wu, L. Zhang, J. Jia, T. Wang, R. Shu, Z. He, and J. Wang, "Polarization-Maintaining Design for Satellite-Based Quantum Communication Terminals," *Optics Express*, vol. 28, no. 8, pp. 10 746–10 759, 2020.
- [35] L. Bassett, "Quantum Mechanics With Applications to Nanotechnology and Information Science," *Physics Today*, vol. 67, no. 7, pp. 50–50, 2014.
- [36] N. C. Pistoni, "Simplified Approach to the Jones Calculus in Retracing Optical Circuits," *Applied optics*, vol. 34, no. 34, pp. 7870–7876, 1995.
- [37] M. Toyoshima, H. Takenaka, Y. Shoji, Y. Takayama, M. Takeoka, M. Fujiwara, and M. Sasaki, "Polarization-Basis Tracking Scheme in Satellite Quantum Key Distribution," *International Journal of Optics*, vol. 2011, no. 1, p. 254154, 2011.
- [38] J. Tayebi, T. Chen, and H. Wang, "Dynamics and Control of Flexible Satellite Using Reaction Sphere Actuators," *Space: Science & Technology*, vol. 3, p. 0077, 2023.
- [39] R. L. Fante, "Electromagnetic Beam Propagation in Turbulent Media," *Proceedings of the IEEE*, vol. 63, no. 12, pp. 1669–1692, 2005.
- [40] —, "Electromagnetic Beam Propagation in Turbulent Media: an Update," *Proceedings of the IEEE*, vol. 68, no. 11, pp. 1424–1443, 2005.
- [41] M. A. Nielsen and I. L. Chuang, *Quantum Computation and Quantum Information*. Cambridge university press, 2010.
- [42] A. de Oliveira, E. Diamond-Hitchcock, D. Walker, M. Wells-Pestell, G. Pelegri, C. Picken, G. Malcolm, A. Daley, J. Bass, and J. Pritchard, "Demonstration of Weighted-Graph Optimization on a Rydberg-Atom Array Using Local Light Shifts," *PRX Quantum*, vol. 6, no. 1, p. 010301, 2025.
- [43] M.-T. Nguyen, J.-G. Liu, J. Wurtz, M. D. Lukin, S.-T. Wang, and H. Pichler, "Quantum Optimization With Arbitrary Connectivity Using Rydberg Atom Arrays," *PRX Quantum*, vol. 4, no. 1, p. 010316, 2023.
- [44] M. F. Serret, B. Marchand, and T. Ayril, "Solving Optimization Problems With Rydberg Analog Quantum Computers: Realistic Requirements for Quantum Advantage Using Noisy Simulation and Classical Benchmarks," *Physical Review A*, vol. 102, no. 5, p. 052617, 2020.
- [45] C. H. Bennett, G. Brassard, S. Popescu, B. Schumacher, J. A. Smolin, and W. K. Wootters, "Purification of Noisy Entanglement and Faithful Teleportation via Noisy Channels," *Physical review letters*, vol. 76, no. 5, p. 722, 1996.
- [46] Y. Li, W.-Q. Cai, J.-G. Ren, C.-Z. Wang, M. Yang, L. Zhang, H.-Y. Wu, L. Chang, J.-C. Wu, B. Jin *et al.*, "Microsatellite-based Real-Time Quantum Key Distribution," *Nature*, pp. 1–8, 2025.
- [47] L. Zhang, J. Dai, C. Li, J. Wu, J. Jia, and J. Wang, "Design and In-orbit Test of a High Accuracy Pointing Method in Satellite-to-Ground Quantum Communication," *Optics express*, vol. 28, no. 6, pp. 8291–8307, 2020.
- [48] D. R. Gozzard, S. Walsh, and T. Weinhold, "Vulnerability of Satellite Quantum Key Distribution to Disruption From Ground-Based Lasers," *Sensors*, vol. 21, no. 23, p. 7904, 2021.
- [49] V. D. Tubío, M. B. Aldecocea, J. van Dam, A. Sørensen, and J. Borregaard, "Satellite-Assisted Quantum Communication With Single Photon Sources and Atomic Memories," *arXiv preprint arXiv:2411.09533*, 2024.
- [50] C. J. Dennehy and O. S. Alvarez-Salazar, "A Survey of the Spacecraft Line-of-Sight Jitter Problem," in *AAS Annual Guidance and Control Conference*, no. NF1676L-32261, 2019.

$$R_{\text{pre}}(t; \lambda) = p_{\text{util}} \cdot P_{\text{accept}}^{\text{pre}}(t; \lambda) \cdot P(\text{link available} \mid \text{accepted}) \quad (87)$$

$$\begin{aligned} P(\text{link available} \mid \text{accepted}) &= \frac{P_{\text{stored}}^{\text{pre}}(t; \lambda)}{P_{\text{accept}}^{\text{pre}}(t; \lambda)} \cdot 1 + \frac{P_{\{0\}}^{\text{pre}}(t; \lambda)}{P_{\text{accept}}^{\text{pre}}(t; \lambda)} \cdot [1 - (1 - p')^{G_{\text{max}}}] \\ &= \frac{P_{\text{stored}}^{\text{pre}}(t; \lambda) + P_{\{0\}}^{\text{pre}}(t; \lambda) [1 - (1 - p')^{G_{\text{max}}}]}{P_{\text{accept}}^{\text{pre}}(t; \lambda)} \end{aligned} \quad (88)$$

$$(89)$$

$$R_{\text{pre}}(t; \lambda) = p_{\text{util}} \cdot \left\{ P_{\text{stored}}^{\text{pre}}(t; \lambda) + P_{\{0\}}^{\text{pre}}(t; \lambda) [1 - (1 - p')^{G_{\text{max}}}] \right\}. \quad (90)$$